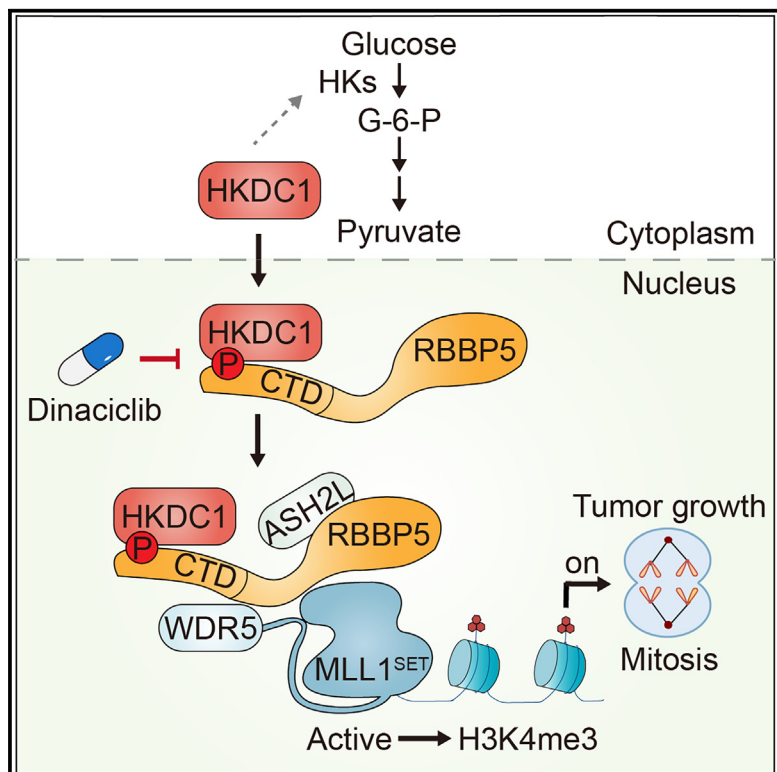


## Nuclear-localized HKDC1 promotes hepatocellular carcinoma through phosphorylating RBBP5 to upregulate H3K4me3

### Graphical abstract



### Authors

Ling Ye, Shengqi Shen, Qiankun Mao, ..., Shi-ting Li, Ping Gao, Huafeng Zhang

### Correspondence

pgao2@ustc.edu.cn (P.G.), hzhang22@ustc.edu.cn (H.Z.)

### In brief

Ye et al. uncover that nuclear-localized HKDC1 functions as a protein kinase and promotes hepatocellular carcinoma (HCC) progression by phosphorylating RBBP5, facilitating MLL1 complex assembly, and upregulating H3K4me3. They identify elevated levels of HKDC1 and phosphorylated RBBP5 as potential therapeutic targets and prognostic biomarkers for HCC.

### Highlights

- Nuclear-localized HKDC1 functions as a protein kinase and phosphorylates RBBP5
- HKDC1-mediated RBBP5 phosphorylation promotes MLL1 complex assembly
- HKDC1 promotes mitosis-related gene expression and cell proliferation
- Targeting HKDC1 protein kinase activity retards liver tumor growth



## Article

# Nuclear-localized HKDC1 promotes hepatocellular carcinoma through phosphorylating RBBP5 to upregulate H3K4me3

Ling Ye,<sup>1,6</sup> Shengqi Shen,<sup>5,6</sup> Qiankun Mao,<sup>1</sup> Hui Lu,<sup>1</sup> Haiying Liu,<sup>1</sup> Pinggen Zhang,<sup>1</sup> Zetan Jiang,<sup>1,2</sup> Wenhao Ma,<sup>1</sup> Yuchen Sun,<sup>1</sup> Yiyang Chu,<sup>1</sup> Zilong Zhou,<sup>1</sup> Rui Liu,<sup>1</sup> Jian Li,<sup>1</sup> Shi-ting Li,<sup>5</sup> Ping Gao,<sup>5,\*</sup> and Huafeng Zhang<sup>1,2,3,4,7,\*</sup>

<sup>1</sup>Department of General Surgery, The First Affiliated Hospital of USTC, Division of Life Sciences and Medicine, University of Science and Technology of China, Hefei 230027, China

<sup>2</sup>Key Laboratory of Immune Response and Immunotherapy, School of Basic Medical Sciences, Division of Life Science and Medicine, University of Science and Technology of China, Hefei 230027, China

<sup>3</sup>Institute of Health and Medicine, Hefei Comprehensive National Science Center, Hefei 230601, China

<sup>4</sup>Anhui Key Laboratory of Molecular Oncology, Hefei 230026, China

<sup>5</sup>Medical Research Institute, Guangdong Provincial People's Hospital, Guangdong Academy of Medical Sciences, Southern Medical University, Guangzhou 510080, China

<sup>6</sup>These authors contributed equally

<sup>7</sup>Lead contact

\*Correspondence: pgao2@ustc.edu.cn (P.G.), hzhang22@ustc.edu.cn (H.Z.)

<https://doi.org/10.1016/j.celrep.2025.115250>

## SUMMARY

Metabolic enzymes play significant roles in the pathogenesis of various cancers through both canonical and noncanonical functions. Hexokinase domain-containing protein 1 (HKDC1) functions beyond glucose metabolism, but its underlying mechanisms in tumorigenesis are not fully understood. Here, we demonstrate that nuclear-localized HKDC1 acts as a protein kinase to promote hepatocellular carcinoma (HCC) cell proliferation. Mechanistically, HKDC1 phosphorylates RB binding protein 5 (RBBP5) at Ser497, which is crucial for MLL1 complex assembly and subsequent histone H3 lysine 4 trimethylation (H3K4me3) modification. This leads to the transcriptional activation of mitosis-related genes, thereby driving cell cycle progression and proliferation. Notably, targeting HKDC1's protein kinase activity, but not its HK activity, blocks RBBP5 phosphorylation and suppresses tumor growth. Clinical analysis further reveals that RBBP5 phosphorylation positively correlates with HKDC1 levels and poor HCC prognosis. These findings highlight the protein kinase function of HKDC1 in the activation of H3K4me3, gene expression, and HCC progression.

## INTRODUCTION

Metabolic reprogramming, a hallmark of cancer, allows tumor cells to engage in abnormal processes, including highly activated glycolysis with aberrant enzyme expression, regardless of oxygen availability. This phenomenon, known as the Warburg effect, ultimately leads to increased cell proliferation and cancer progression.<sup>1,2</sup> Recent studies have revealed that many glycolytic enzymes acquire noncanonical functions and regulate gene expression by acting as protein kinases.<sup>3,4</sup> For instance, pyruvate kinase M2 (PKM2) promotes tumorigenesis by inducing the expression of cyclin D1 and c-Myc through phosphorylating histone H3.<sup>5</sup> Similarly, 6-phosphofructo-2-kinase/fructose-2,6-biphosphatase 4 (PFKFB4) directly phosphorylates SRC-3 and transcriptionally activates SRC-3-mediated tumor metastasis.<sup>6</sup> Additionally, PKM2 functions as a protein kinase when dimerizing<sup>7</sup> or when acetylated by p300.<sup>8</sup> Consequently, strategies that promote the dimer-tetramer transition or inhibit p300 have emerged as promising therapies to restrict tumor cell proliferation. Thus, metabolic

enzymes with noncanonical functions not only confer growth advantages for cancer progression but also offer novel therapeutic strategies. These strategies could address limitations associated with targeting owing to the classical housekeeping activities of these enzymes. Nevertheless, it remains unclear whether other metabolic enzymes exhibit noncanonical functions in tumorigenesis.

Hexokinase (HK) is the first rate-limiting enzyme in the glycolytic pathway. It uses ATP as a donor to phosphorylate glucose and generate glucose-6-phosphate. The HK family includes five members: HK1–4 and HK domain-containing protein 1 (HKDC1). Among these, HK2 is frequently overexpressed in various cancers, enhancing glycolytic flux and tumor growth.<sup>9,10</sup> Recent research has highlighted its protein kinase activity in regulating nuclear factor κB (NF-κB)-mediated PD-L1 expression by phosphorylating and degrading IκBα, which contributes to tumor immune escape.<sup>11</sup> HKDC1, another member of the HK family, is also highly expressed during tumorigenesis. In breast cancer, HKDC1 interacts with voltage-dependent anion channel 1 (VDAC1) on the outer mitochondrial membrane. This



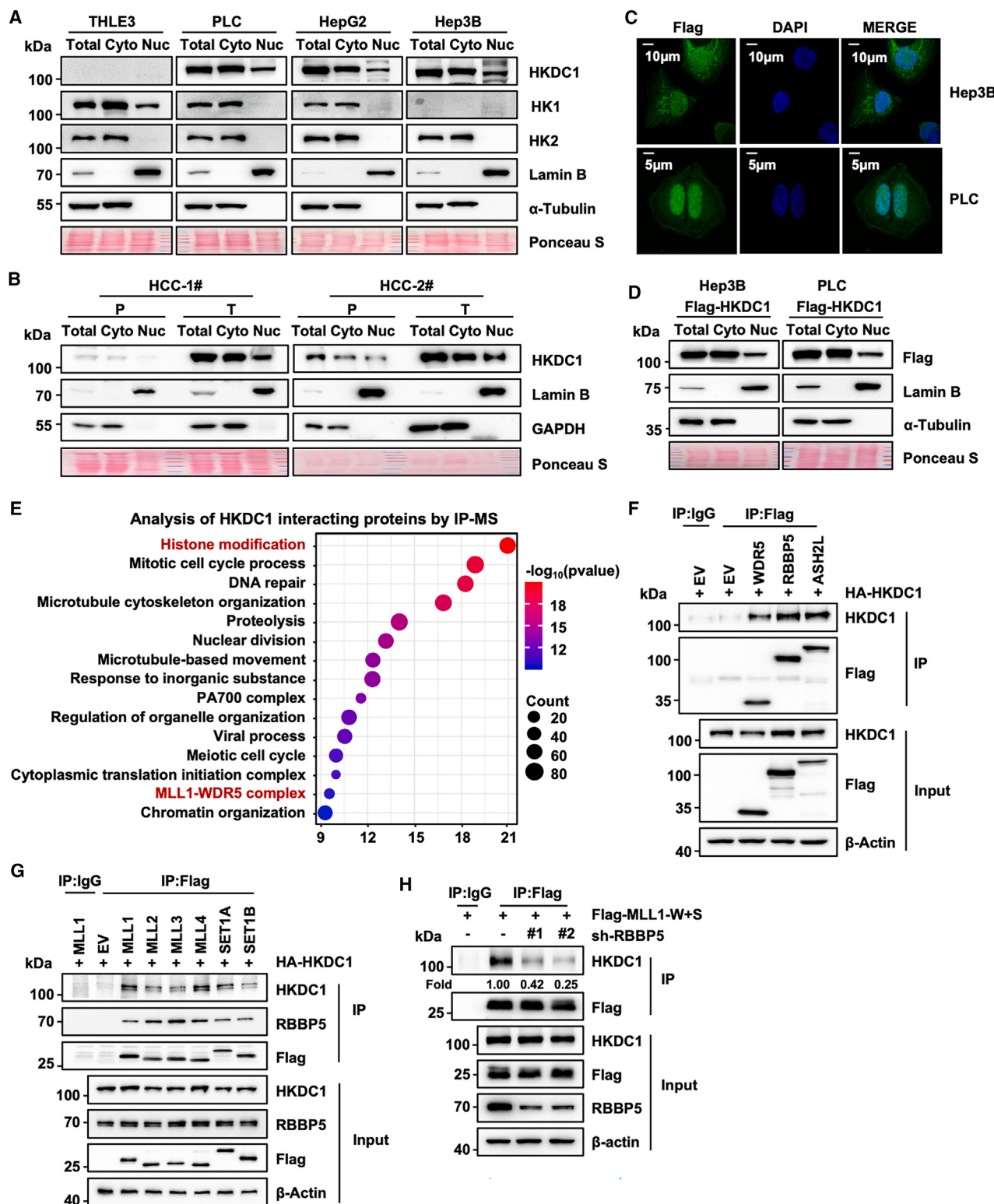


**Figure 1. Nuclear-localized HKDC1 interacts with the MLL1 complex**

(A) Western blot analysis of the localization of endogenous HKDC1, HK1, and HK2 in THLE3, PLC, HepG2, and Hep3B cells. Lamin B and  $\alpha$ -tubulin served as markers for nuclear (Nuc) and cytosolic (Cyto) proteins, respectively. Ponceau staining served as a loading control.

(legend continued on next page)

interaction increases the mitochondrial membrane potential and glucose uptake, supporting tumor growth.<sup>12</sup> Moreover, disrupting the HKDC1-VDAC1 interaction inhibits the proliferation of extranodal nasal-type natural killer/T cell lymphoma (ENKTL), suggesting a potential therapeutic strategy.<sup>13</sup> Interestingly, HKDC1 exhibits lower HK activity than other family members,<sup>14</sup> indicating that HKDC1 may have nonmetabolic functions. Our previous research revealed that in hepatocellular carcinoma (HCC) cells, HKDC1 binds to the cytoskeleton protein ACTA2 and presents STAT1 to IFNGR1 upon interferon (IFN)- $\gamma$  stimulation. This interaction occurs independently of HKDC1's metabolic function and leads to STAT1 activation, PD-L1 expression, and tumor immune evasion.<sup>15</sup> These early findings prompted us to further investigate the noncanonical functions of HKDC1 in tumor progression.

Epigenomic dysregulation drives abnormal transcriptional processes, which promote cancer onset and progression. Extensive research has shown that both global and local changes in histone methylation are key features of cancer cells. Pathogenic signals target the expression or activity of methyltransferases and demethylases, leading to disruptions in gene expression and genome integrity.<sup>16</sup> For example, mutations in p53 in HCC cause aberrant expression of these modifiers and transcriptional activation.<sup>17</sup> Most histone methyltransferases, such as KMT2A (also known as mixed lineage leukemia 1 [MLL1]), function by forming a core complex.<sup>18,19</sup> Studies have reported that inhibiting the assembly of this complex restricts transcriptional dysregulation and tumor growth by affecting its catalytic activity and downstream histone methylation.<sup>20,21</sup> Despite the crucial role of histone methylation in cancer progression, relatively little is known about how methyltransferases are altered and whether other oncoproteins are involved.

In this study, we comprehensively characterized the protein kinase function of HKDC1 in accelerating HCC progression. We found that HKDC1, through its protein kinase function rather than its HK activity, phosphorylates RB binding protein 5 (RBBP5). This phosphorylation promotes the assembly of the MLL1 complex, which in turn increases H3K4me3 levels and stimulates the expression of mitosis-related genes, ultimately driving tumor progression. Our findings suggest a potential therapeutic approach that targets the protein kinase activity of HKDC1 in liver cancer.

## RESULTS

### Nuclear-localized HKDC1 interacts with the MLL1 complex

To investigate the role of HKDC1 in tumor cell proliferation and liver cancer progression, we first established an NRAS/shp53-induced HCC model in wild-type (WT) or *HKDC1*<sup>-/-</sup> mice. Our results demonstrated that HKDC1 knockout significantly reduced both the incidence of liver cancer and tumor growth (Figure S1A). Despite the high homology of HKDC1 with HK1 and HK2, HK assays in Hep3B cells showed that its catalytic activity was much lower (Figure S1B), as previously reported. These findings suggest that HKDC1 plays a crucial role beyond glucose metabolism in driving HCC progression. To further explore the noncanonical functions of HKDC1 in tumor growth, we conducted a tumor xenograft assay in immunodeficient mice by subcutaneously injecting Hep3B cells that overexpressed either WT HKDC1 or a catalytic site mutant (S602A).<sup>15</sup> Both WT HKDC1 and the S602A mutant stimulated tumor growth (Figure S1C). These results indicate that HKDC1 has additional functions, independent of its enzymatic activity or immune regulation, that contribute to tumor progression.

Compelling studies have reported that metabolic enzymes can acquire noncanonical functions when their subcellular localization changes. To determine whether HKDC1 exhibits subcellular-compartment-dependent functions, we first examined localization through subcellular fractionation. Our results showed that HKDC1, unlike HK1 or HK2, exhibits nuclear localization in PLC/PRF/5 (PLC), HepG2, and Hep3B cells (Figure 1A). We also observed aberrant HKDC1 expression in HCC cells compared with normal liver THLE3 cells (Figure S1D). Similar results were observed in A549 and CALU3 lung cancer cells, as well as MDA-MB-231 and MDA-MB-468 breast cancer cells (Figure S1E). Additionally, we investigated the intracellular distribution of HKDC1 in clinical HCC tissues. We found that endogenous HKDC1 is distributed in the nucleus and that both total and nuclear HKDC1 levels are significantly greater in tumor tissues than in paracancerous tissues (Figure 1B). We then confirmed that exogenous FLAG-tagged HKDC1 colocalized with the nucleus through immunofluorescence analysis in Hep3B and PLC cells (Figure 1C), which aligns with the western blot results (Figure 1D). Together, these data indicate that HKDC1 exhibits nuclear localization with aberrant expression in HCC.

- (B) Western blot analysis of the localization of endogenous HKDC1 in paired human adjacent noncancerous liver tissues (P) and HCC tissues (T). Lamin B and GAPDH served as markers for the Nuc and Cyto proteins, respectively. Ponceau staining served as a loading control.
- (C) Immunofluorescence images showing the colocalization of FLAG-HKDC1 (green) and the nucleus (blue) in Hep3B and PLC cells. HKDC1 proteins were stained with FLAG, and nuclei were stained with DAPI. Scale bars, 10  $\mu$ m and 5  $\mu$ m.
- (D) Western blot analysis of the localization of exogenous FLAG-tagged HKDC1 in Hep3B and PLC cells. Lamin B and  $\alpha$ -tubulin served as markers for the Nuc and Cyto proteins, respectively. Ponceau staining served as a loading control.
- (E) Immunoprecipitation-mass spectrometry (IP-MS) and pathway enrichment analysis of HKDC1-interacting proteins in PLC cells expressing FLAG-HKDC1 via Metascape. IP was performed via the use of an anti-FLAG antibody following the separation of Nuc components.
- (F) HEK293T cells were transfected with hemagglutinin (HA)-HKDC1 and FLAG-WDR5, RBBP5, or ASH2L plasmids, followed by IP using an anti-FLAG antibody or immunoglobulin (Ig)G and western blotting. Empty vector (EV) was used as a control.
- (G) HEK293T cells were transfected with HA-HKDC1 and FLAG-MLL protein-W+S (WDR5 Interaction [WIN] motif and Su(var)3-9, enhancer-of-zeste, and trithorax [SET] domain) plasmids, followed by IP using an anti-FLAG antibody or IgG and western blotting.
- (H) Hep3B cells stably overexpressing FLAG-MLL1-W+S were further infected with viruses expressing NTC (non-target control), sh-RBBP5#1, or sh-RBBP5#2, followed by IP using an anti-FLAG antibody or IgG and western blotting. The “–” indicates the NTC-infected control group for sh-RBBP5 knockdown. See also Figure S1.

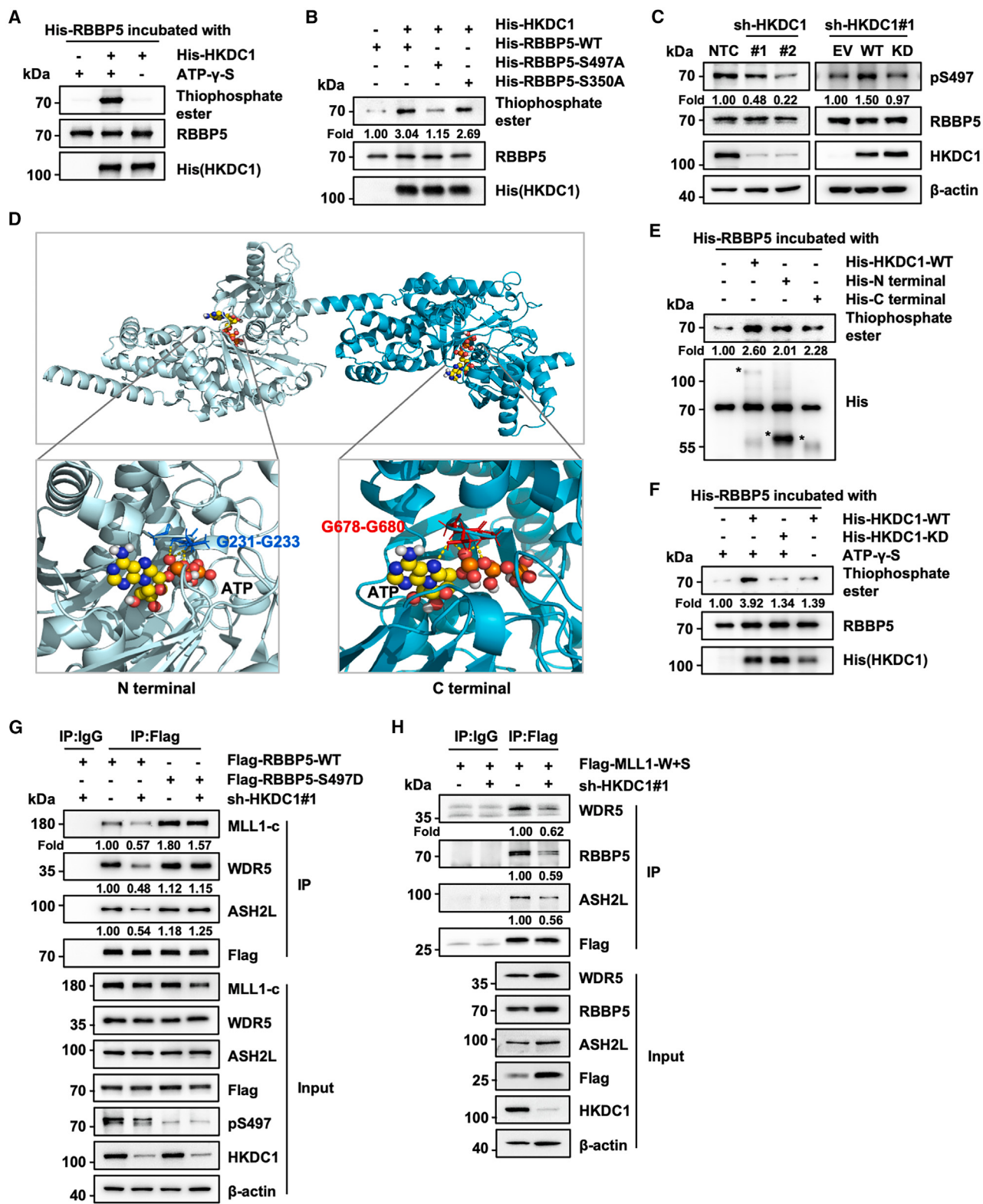


**Figure 2. HKDC1 phosphorylates RBBP5 at Ser497 and promotes MLL1 complex assembly**

(A) Bacterially purified His-RBBP5 was incubated with or without His-HKDC1 proteins in the presence of ATP- $\gamma$ -S for an *in vitro* kinase assay.

(B) Bacterially purified His-tagged WT RBBP5, the S350A mutant, or the S497A mutant was incubated with or without His-HKDC1 proteins in the presence of ATP- $\gamma$ -S for an *in vitro* kinase assay.

*(legend continued on next page)*

To further characterize the role of nuclear-localized HKDC1, we stably expressed FLAG-tagged HKDC1 in PLC cells and conducted mass spectrometry analysis after immunoprecipitating the nuclear fraction. This analysis identified a series of nuclear proteins that interact with HKDC1, including components of the MLL1-WDR5 complex, which are associated with histone modification (Figure 1E). The MLL complexes consist of six diverse MLL proteins and various interacting proteins, sharing some common subunits. Notably, WDR5, RBBP5, and ASH2L form a core entity that alters the conformation of MLL proteins and enhances their otherwise weak activity in methylating histone H3 on lysine 4 (H3K4).<sup>18,19,22</sup> We then investigated whether HKDC1 interacts with the MLL complex. Coimmunoprecipitation assays in 293T cells demonstrated that HKDC1 interacts with WDR5, RBBP5, and ASH2L (Figure 1F). Furthermore, *in vitro* pull-down assays revealed that HKDC1 directly binds to RBBP5 (Figure S1F). This interaction was confirmed by immunoprecipitating nuclear FLAG-tagged HKDC1, showing that endogenous RBBP5 associates with nuclear HKDC1 in Hep3B cells (Figure S1G). Since RBBP5 is a common and essential subunit of the MLL complexes, we observed that HKDC1 interacts with all six MLL family proteins in 293T cells (Figure 1G). However, in HCC, MLL1 exhibits increased expression with rare mutations,<sup>23–26</sup> making it preferentially interact with HKDC1 (Figure 1E). Additionally, the knockdown of RBBP5 reduced the interaction between HKDC1 and MLL1 (Figure 1H), suggesting that HKDC1 interacts with MLL1 through its direct binding to RBBP5. Taken together, these results indicate that nuclear-localized HKDC1 interacts with the MLL1 complex by directly binding to RBBP5 in HCC.

### HKDC1 phosphorylates RBBP5 at Ser497 and promotes MLL1 complex assembly

Reports indicate that metabolic enzymes, such as PKM2,<sup>5</sup> PGK1,<sup>27</sup> and PCK1,<sup>28</sup> which transfer a phosphate group from ATP to a metabolite, acquire protein kinase activity during cancer progression. To investigate the function of nuclear HKDC1 on RBBP5, we first carried out an *in vitro* protein phosphorylation assay by incubating purified, bacterially expressed His-RBBP5 and His-HKDC1 with or without ATP-γ-S. The results demonstrated that HKDC1 phosphorylates RBBP5 (Figure 2A). Moreover, knocking down HKDC1 in Hep3B cells reduced the phosphorylation of the serine residue of RBBP5 (Figure S2A). To identify the specific phosphorylation site on RBBP5, we purified His-tagged WT RBBP5 and mutants S350A and S497A, which were predicted phosphorylation sites according to the online database at [www.phosphosite.org](http://www.phosphosite.org). *In vitro* protein kinase assay

revealed that the S497A mutant was not phosphorylated by HKDC1, indicating that Ser497 is the phosphorylation site (Figure 2B). This finding was further confirmed by an immunoprecipitation assay in Hep3B cells. Here, knocking down HKDC1 reduced the phosphorylation of WT RBBP5 but did not affect the S497A mutant (Figure S2B). Next, we generated an antibody that specifically recognizes Ser497-phosphorylated RBBP5 (pS497). We verified the specificity of the antibody through dot blot and immunoprecipitation assays (Figures S2C and S2D). Western blot analysis using this antibody showed that the pS497 level decreased upon suppression of HKDC1 (Figure 2C). Consistently, overexpression of WT HKDC1 following endogenous HKDC1 knockdown increased the pS497 level, while expressing the kinase-dead (KD) mutant remained stable (Figure 2C). These results confirmed that HKDC1 functions as a protein kinase and phosphorylates RBBP5 at the Ser497 residue.

Protein kinases transfer a phosphate group from ATP to a protein substrate and share a conserved structure with a regulatory domain and a catalytic domain.<sup>29</sup> The catalytic domain includes a small lobe, a large lobe, and a docking pocket between these lobes, which contains ATP and protein substrate binding sites.<sup>30</sup> To investigate the active center and working model of HKDC1, we used AlphaFold2 to predict its protein structure and identify potential active sites. Intriguingly, we observed that HKDC1 has nearly symmetrical structures at both the N and C termini, with a docking pocket between the small and large lobes (Figure 2D). Molecular docking predictions revealed that the binding sites of ATP at both termini feature a glycine-rich motif (Gly-Thr-Gly [GTG]) (Figure 2D) that is structurally similar to the glycine-rich loop in classical kinases that facilitates ATP binding.<sup>30</sup> These findings suggest that the GTG motifs in both terminals may serve as potential active sites for HKDC1. We then constructed HKDC1 truncations of the N- and C-termini as well as a KD mutant in which the two GTG motifs were mutated to alanines (AAAs). *In vitro* kinase assays demonstrated that both the N- and C-termini exhibit protein kinase activity (Figure 2E). The results from *in vitro* assays (Figure 2F) and cell line experiments (Figure 2C) revealed that WT HKDC1, but not the KD mutant, promoted the phosphorylation of RBBP5, suggesting that the GTG motifs are crucial for HKDC1's protein kinase activity. These data support the conclusion that HKDC1 possesses protein kinase function, with the GTG motifs in both the N and C termini serving as the active sites.

Previous studies have shown that RBBP5, in conjunction with WDR5 and ASH2L, forms a core entity that interacts stably with MLL enzymes and enhances their otherwise weak activity.<sup>18,31</sup>

(C) Western blot analysis of pS497 levels in Hep3B cells stably expressing NTC (non-target control), sh-HKDC1#1, or sh-HKDC1#2 and Hep3B cells over-expressing EV, WT HKDC1, or the KD (kinase-dead) mutant following knockdown of endogenous HKDC1 via sh-HKDC1#1.

(D) Molecular docking model of HKDC1 with ATP.

(E) Bacterially purified His-RBBP5 was incubated with His-tagged WT HKDC1 or N-terminal (1–470 aa) or C-terminal (465–917 aa) proteins in the presence of ATP-γ-S for an *in vitro* kinase assay.

(F) Bacterially purified His-RBBP5 was incubated with His-tagged WT HKDC1 or the KD mutant proteins in the presence of ATP-γ-S for an *in vitro* kinase assay.

(G) Hep3B cells stably overexpressing FLAG-tagged WT RBBP5 or the S497D mutant were further infected with viruses expressing NTC or sh-HKDC1#1, followed by immunoprecipitation using an anti-FLAG antibody or IgG and western blotting.

(H) Hep3B cells stably expressing FLAG-MLL1-W+S (WIN and SET domains) were further infected with viruses expressing NTC or sh-HKDC1#1, followed by immunoprecipitation using an anti-FLAG antibody or IgG and western blotting.

See also Figure S2.

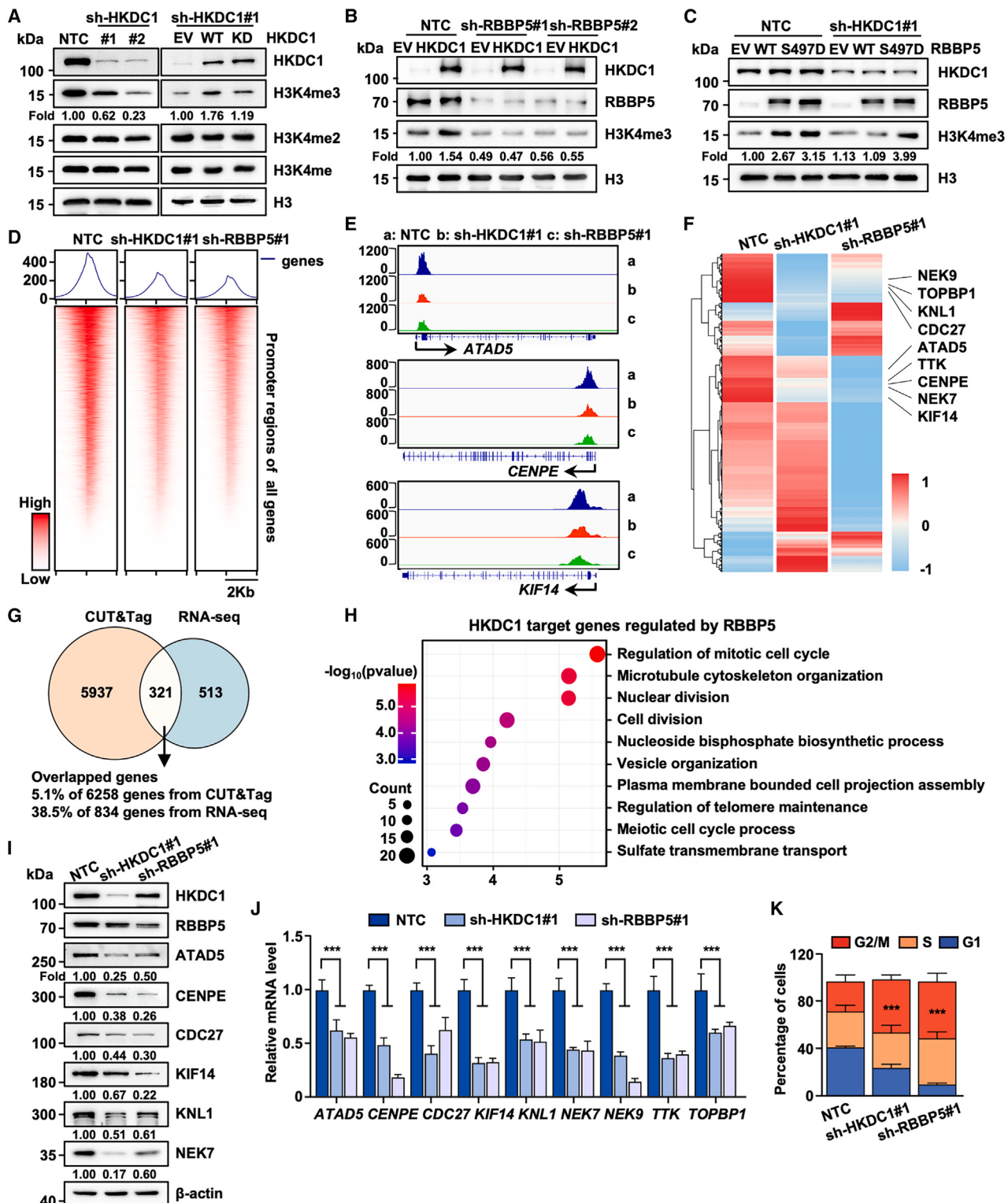


**Figure 3. HKDC1-mediated phosphorylation of RBBP5 upregulates H3K4me3 to increase the expression of mitosis-related genes**

(A) Western blot analysis of the indicated histone methylation markers in Hep3B cells infected with viruses expressing NTC, sh-HKDC1#1, or sh-HKDC1#2 and Hep3B cells overexpressing WT HKDC1 or the KD mutant following knockdown of endogenous HKDC1 via sh-HKDC1#1.

(B) Western blot analysis of the H3K4me3 level in Hep3B cells infected with viruses expressing NTC, sh-RBBP5#1, or sh-RBBP5#2 following overexpression of HKDC1.

*(legend continued on next page)*

The role of RBBP5 in the assembly and regulation of the MLL1 complex has become clear. The C-terminal distal (CTD) domain of RBBP5 helps maintain the compact conformation of the MLL1 complex.<sup>32</sup> Since Ser497 of RBBP5 is located in this CTD domain, we hypothesized that HKDC1-mediated phosphorylation of Ser497 is crucial for MLL1 complex assembly. To test this hypothesis, we performed an immunoprecipitation assay in Hep3B cells overexpressing WT RBBP5, the S497A mutant (a nonphosphorylatable alanine substitution), or the S497D mutant (a phosphomimetic). The results revealed that, unlike WT RBBP5 or the S497D mutant, only the S497A mutant failed to promote the interaction between RBBP5 and other components of the MLL1 core complex (Figure S2E). These findings suggest that the phosphorylation of RBBP5 at Ser497 is essential for proper assembly of the MLL1 complex.

Furthermore, we observed that knocking down HKDC1 reduced the interaction between RBBP5 and other components of the MLL1 complex without affecting the S497D mutant (Figures 2G and S2F). Additionally, WT HKDC1, but not the KD mutant, facilitated these interactions (Figure S2G). These results indicate that HKDC1-mediated phosphorylation of RBBP5 is crucial for the assembly of the MLL1 complex. To further investigate this phenomenon, we overexpressed the WIN and SET domains of MLL1 and found that HKDC1 knockdown reduced the stability of the MLL1 complex by weakening internal interactions (Figure 2H). We also assessed the role of HKDC1's HK activity in RBBP5 phosphorylation and MLL1 complex assembly through *in vitro* and cell-based experiments. The S602A mutant, which lacks HK activity, had effects similar to those of WT HKDC1 on RBBP5 phosphorylation (Figures S2H and S2I) and MLL1 complex assembly (Figure S2J). These findings suggest that the protein kinase function of HKDC1 operates independently of its HK activity. Furthermore, we examined the binding of HKDC1 to the CTD of RBBP5 via a pull-down assay (Figure S2K). In conclusion, HKDC1 phosphorylates RBBP5 and stabilizes the MLL1 complex.

#### HKDC1-mediated phosphorylation of RBBP5 upregulates H3K4me3 to increase the expression of mitosis-related genes

The MLL family methylates H3K4 to increase genome accessibility and transcription. Since HKDC1 promotes MLL1 complex

assembly, we investigated its role in histone methylation. Our western blot analysis of Hep3B nuclear extracts showed that knocking down or overexpressing HKDC1 significantly reduced or increased H3K4me3 levels, respectively, whereas H3K4me1 and H3K4me2 remained unaffected (Figure 3A). These findings indicate that HKDC1 specifically activates H3K4 trimethylation. Importantly, we demonstrated that the upregulation of H3K4me3 by overexpressing HKDC1 relies on its protein kinase function, not its HK activity (Figures 3A and S3A). Since RBBP5 phosphorylation at the Ser497 site is crucial for H3K4me3 (Figure S3B), we further examined the role of the HKDC1-phosphorylated RBBP5 axis in H3K4me3 by manipulating HKDC1 and RBBP5. Our results revealed that HKDC1-mediated promotion of H3K4me3 was reduced by RBBP5 knockdown, and suppressing HKDC1 after RBBP5 overexpression produced a similar effect (Figures 3B and 3C). Notably, the overexpression of the S497D mutant continued to increase H3K4me3 levels regardless of the presence of HKDC1 (Figure 3C), confirming that HKDC1 facilitates H3K4me3 by phosphorylating RBBP5. In summary, HKDC1 stimulates H3K4me3 through its protein kinase activity on RBBP5 phosphorylation.

To investigate the regulatory effect of HKDC1 on global H3K4me3 modification, we performed a CUT&Tag sequencing assay in PLC cells in which either HKDC1 or RBBP5 was knocked down. As H3K4me3 is predominantly enriched in the promoter-proximal regions,<sup>33,34</sup> we specifically analyzed H3K4me3 signals within  $\pm 2$  kb from the transcription start site (TSS). The heatmap represents the normalized signal distribution of H3K4me3 across these regions (Figure 3D). We identified 6,258 genes whose H3K4me3 levels in promoter regions were significantly reduced (fold change  $> 1.5$ ) upon knockdown of HKDC1 or RBBP5, indicating the co-regulation by HKDC1 and RBBP5 (Figure S3C). IGV images revealed that H3K4me3 levels in the promoter regions of ATAD5, CENPE, and KIF14 were markedly reduced when HKDC1 or RBBP5 was suppressed (Figure 3E). These data demonstrate that HKDC1 and RBBP5 are crucial for H3K4me3 modification in promoter regions. We then conducted an RNA sequencing (RNA-seq) assay in PLC cells with HKDC1 or RBBP5 knocked down to assess their roles in gene transcription. The RNA-seq analysis revealed that knocking down either HKDC1 or RBBP5 repressed the expression of 834 genes (Figure S3D), with the heatmap showing similar

(C) Western blot analysis of the H3K4me3 level in Hep3B cells infected with viruses expressing NTC or sh-HKDC1#1 following overexpressing EV, WT RBBP5, or the S497D mutant.

(D) PLC cells were infected with viruses expressing NTC, sh-HKDC1#1, or sh-RBBP5#1 followed by CUT&Tag sequencing using an anti-H3K4me3 antibody. The heatmap shows the H3K4me3 distribution of all genes within a 2 kb distance from the transcription start site (TSS).

(E) H3K4me3 markers of CUT&Tag tracks for ATAD5, CENPE, and KIF14 in PLC cells were determined via IGV software analysis. a, b, and c represent different conditions (NTC, sh-HKDC1#1, and sh-RBBP5#1) of CUT&Tag data.

(F) PLC cells infected with viruses expressing NTC, sh-HKDC1#1, or sh-RBBP5#1 were subjected to RNA sequencing (RNA-seq) analysis. The heatmap shows the Z scores of genes.

(G) Venn diagram showing overlapping genes co-regulated by HKDC1 and RBBP5 based on the CUT&Tag data and RNA-seq data in PLC cells.

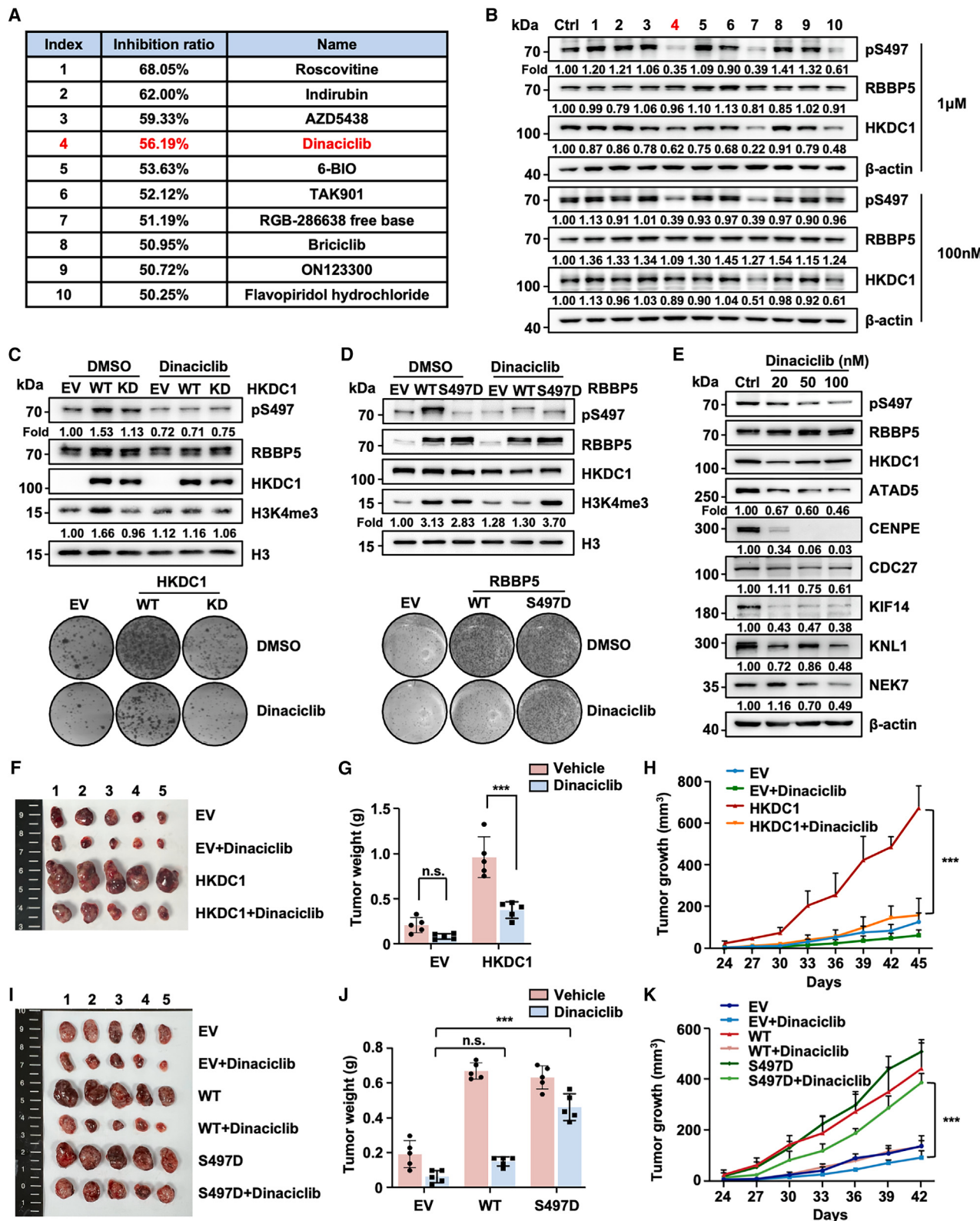
(H) Pathway enrichment analysis of 321 overlapping genes in (G) via Metascape.

(I) Western blot analysis of indicated proteins in Hep3B cells stably expressing NTC, sh-HKDC1#1, or sh-RBBP5#1.

(J) Quantitative real-time PCR (real-time qPCR) analysis of indicated genes in Hep3B cells stably expressing NTC, sh-HKDC1#1, or sh-RBBP5#1 ( $n = 3$  biological replicates).

(K) Cell cycle analysis of Hep3B cells stably expressing NTC, sh-HKDC1#1, or sh-RBBP5#1. G1, S, and G2/M phases are indicated in blue, orange, and red, respectively ( $n = 3$  biological replicates).

Data are presented as mean  $\pm$  SD (J and K). Statistical significance was determined by one-way ANOVA (J and K). See also Figure S3.



(legend on next page)

results (Figure 3F). Interestingly, the H3K4me3 level of 38.5% of these genes (321 genes) was regulated by HKDC1 and RBBP5 (Figure 3G), suggesting that the HKDC1-RBBP5 axis promotes gene expression by increasing H3K4me3 levels in promoter regions.

We explored the biological function of HKDC1-RBBP5-regulated genes by conducting a Gene Ontology (GO) term enrichment analysis of the 321 genes. This analysis revealed that these overlapping genes are primarily involved in mitosis (Figure 3H). A chromatin immunoprecipitation (ChIP) assay confirmed that depleting HKDC1 or RBBP5 reduced H3K4me3 levels in the promoter regions of these mitosis-related genes (Figure S3E). We further examined the expression of some of these genes after knocking down HKDC1 or RBBP5 in Hep3B cells. Both western blot and real-time qPCR assays revealed significant repression of these genes (Figures 3I and 3J). Moreover, overexpressing WT HKDC1 increased the expression of these genes, whereas the KD mutant had no effect (Figures S3F and S3G). Additionally, overexpressing the S602A mutant showed similar results to WT HKDC1 (Figures S3H and S3I). These data suggest that HKDC1 activates H3K4me3 and gene transcription through its protein kinase function. To understand the impact on mitosis-related gene expression, we analyzed cell cycle progression after silencing HKDC1 or RBBP5 in Hep3B cells. The results revealed that these cells arrested in the G2/M phase, indicating the role of HKDC1 and RBBP5 in promoting cell division (Figure 3K). In conclusion, HKDC1-mediated RBBP5 phosphorylation and H3K4me3 activation stimulate gene expression and cell cycle progression.

#### Targeting the HKDC1-RBBP5-H3K4me3 axis retards tumor progression

Protein kinases have emerged as crucial drug targets in current research, particularly in cancer, owing to their essential roles in signal transduction.<sup>35</sup> Given that HKDC1 is a newly identified protein kinase, the exploration of small-molecule inhibitors that target this kinase is promising. We analyzed the phosphorylation site of RBBP5 and found that the Ser497 residue is evolutionarily conserved (Figure S4A). Notably, the phosphorylated peptide features a Ser-Pro motif, which is similar to the target sequence of cyclin-dependent kinases (CDKs) (Figure S4A). This similarity suggests that HKDC1 might be a proline-directed kinase and

could be inhibited by CDK inhibitors. Considering the efficiency of *in vitro* assays and the complexity of the cellular environment, we combined an *in vitro* kinase inhibitor library screening with validation assays in cell lines. For the *in vitro* screening, purified HKDC1, RBBP5, and ATP were incubated with 63 CDK inhibitors from the compound library at a single concentration. We then used a luminescent ADP detection assay to measure the luminescence of the produced ADP (Figure S4B). The reduction in luminescence compared with that of the control indicated the efficiency of each inhibitor against HKDC1, and the top 10 inhibitors are listed in the table shown in Figure 4A. For further validation, we treated Hep3B cells with these candidate inhibitors at low concentrations. Treatment with either 1 μM or 100 nM dinaciclib significantly reduced the phosphorylation of RBBP5 without affecting the levels of endogenous HKDC1 and RBBP5 (Figure 4B). These results suggest that dinaciclib, a selective CDK inhibitor, is a potential inhibitor of HKDC1.

To evaluate the effect of dinaciclib on HKDC1, we used AlphaFold2 to construct a molecular docking model. The results showed that dinaciclib interacts with T232-G233 in the N termini and T679 in the C termini, similar to the GTG motif of HKDC1 where ATP binds (Figure S4C). These findings suggest that dinaciclib acts as an ATP-competitive inhibitor of HKDC1. To confirm that dinaciclib targets the protein kinase function of HKDC1, we treated Hep3B cells overexpressing WT HKDC1 or the KD mutant with dinaciclib. Our results revealed that dinaciclib treatment reduced the pS497 level and inhibited the promotion of H3K4me3 and cell proliferation by WT HKDC1, whereas the KD mutant remained at a low level (Figure 4C). Similarly, dinaciclib treatment diminished the stimulation of H3K4me3 and tumor cell growth by WT RBBP5 without affecting the S497D mutant (Figure 4D). Additionally, dinaciclib suppressed the expression of mitosis-related genes in a dose-dependent manner (Figure 4E). In summary, dinaciclib effectively inhibits HKDC1 protein kinase activity and represses RBBP5 phosphorylation.

Dinaciclib, a potent and selective inhibitor of CDK1, CDK2, CDK5, and CDK9<sup>36</sup>, has advanced to phase 3 clinical trials for chronic lymphocytic leukemia (CLL)<sup>37</sup> and is currently being evaluated in phase 2 trials for solid tumors, including non-small cell lung cancer and breast cancer.<sup>38,39</sup> However, its clinical application in liver cancer remains unexplored. Given that

#### Figure 4. Targeting the HKDC1-RBBP5-H3K4me3 axis retards tumor progression

- (A) Purified HKDC1, RBBP5, and ATP were incubated with 63 CDK inhibitors from the compound library at a concentration of 30 μM. Then, a luminescent ADP detection assay was used to measure the luminescence of the produced ADP. The inhibitors that exhibited a ≥50% reduction in luminescence compared to the control are listed in the table.
  - (B) Western blot analysis of pS497 levels in Hep3B cells treated with the inhibitors listed in (A) at a concentration of 1 μM or 100 nM.
  - (C) Western blot analysis of pS497 and H3K4me3 levels and cell growth in Hep3B cells expressing EV, WT HKDC1, or the KD mutant after 20 nM dinaciclib treatment for 48 h.
  - (D) Western blot analysis of pS497 and H3K4me3 and cell growth in Hep3B cells expressing EV, WT RBBP5, or the S497D mutant after 20 nM dinaciclib treatment for 48 h.
  - (E) Western blot analysis of the indicated genes in Hep3B cells after treatment with 20, 50, or 100 nM dinaciclib for 48 h.
  - (F–H) Hep3B cells overexpressing EV or HKDC1 were subcutaneously injected into nude mice ( $n = 5$  male mice per group). The mice were intraperitoneally injected with 20 mg/kg dinaciclib every 3 days beginning 1 week after inoculation. At the end of the experiment, the tumors were excised (F), and tumor weights were measured (G). Tumor sizes were measured beginning 24 days after inoculation (H).
  - (I–K) Hep3B cells overexpressing EV, WT RBBP5, or the S497D mutant were subcutaneously injected into nude mice ( $n = 5$  male mice per group). The mice were intraperitoneally injected with 20 mg/kg dinaciclib every 3 days beginning 1 week after inoculation. At the end of the experiment, the tumors were excised (I), and tumor weights were measured (J). Tumor sizes were measured beginning 24 days after inoculation (K).
- Data are presented as mean ± SD (G, H, J, and K). Statistical significance was determined by two-way ANOVA (G, H, J, and K). See also Figure S4.

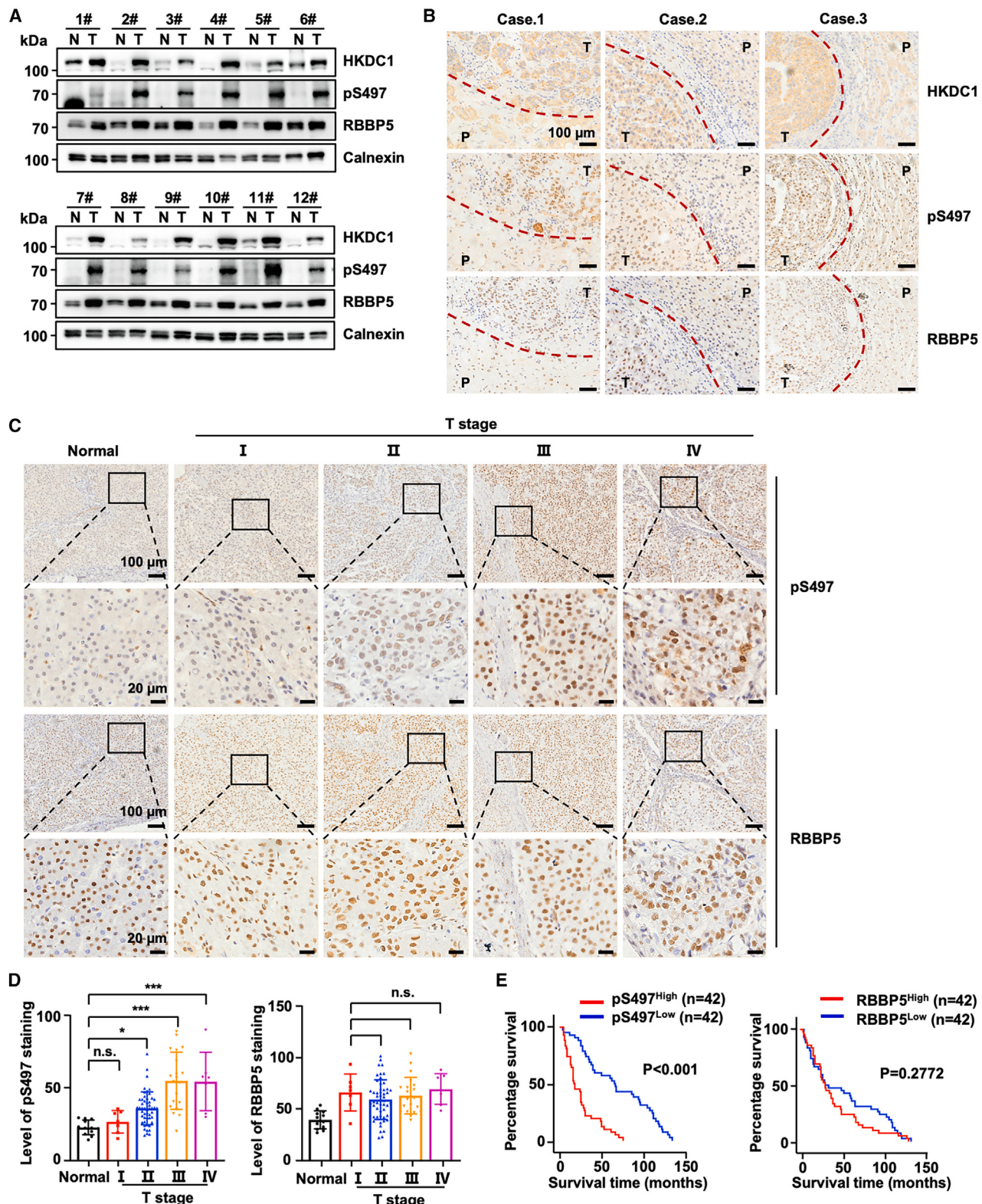


**Figure 5. HKDC1-mediated phosphorylation of RBBP5 correlates with poor prognosis in patients with HCC**

(A) Western blot analysis of HKDC1 and pS497 levels in paired adjacent noncancerous liver tissues (N) and human HCC tissues (T). Calnexin served as a loading control ( $n = 12$  patients with HCC).

(legend continued on next page)

HKDC1 is a significant target of dinaciclib, we assessed its potential for treating HCC with elevated levels of HKDC1 or phosphorylated RBBP5. We conducted xenograft experiments using Hep3B cells stably expressing HKDC1, RBBP5, or the S497D mutant and treated the xenograft-bearing mice with dinaciclib. The results revealed that overexpression of HKDC1, RBBP5, or the S497D mutant accelerated tumor growth (Figures 4F–4K). Importantly, only the S497D mutant continued to grow upon dinaciclib treatment, which is consistent with observations in cell lines (Figures 4I–4K). Western blot analysis of tumor tissue lysates revealed that dinaciclib treatment significantly reduced HKDC1-induced phosphorylation of RBBP5 (Figures S4D and S4E). These data indicated that dinaciclib restricts tumor growth by targeting HKDC1 protein kinase activity. To further demonstrate the role of the HKDC1-RBBP5-H3K4me3 axis in tumor growth, we performed another xenograft experiment using Hep3B cells overexpressing HKDC1 or RBBP5, treated with OICR-9429. This compound disrupts the interaction between MLL1 and WDR5, decreasing the H3K4me3 level.<sup>40</sup> The results showed that OICR-9429 treatment significantly reduced the promotion of tumor cell proliferation by HKDC1 or RBBP5, indicating that the HKDC1-RBBP5-H3K4me3 axis plays a role in tumor progression (Figures S4F–S4H). In summary, targeting HKDC1 protein kinase activity effectively represses tumor growth by disrupting the HKDC1-RBBP5-H3K4me3 axis.

#### **HKDC1-mediated phosphorylation of RBBP5 correlates with poor prognosis in patients with HCC**

Finally, we investigated the pathological significance of our findings in the context of HCC development. We first examined the levels of HKDC1, pS497, and total RBBP5 in 12 paired human HCC tissues and adjacent noncancerous tissues. Western blot analysis revealed that HKDC1 expression was markedly upregulated in HCC tissues compared with matched paracancerous tissues (Figure 5A), which was consistent with our previous study.<sup>15</sup> Moreover, phosphorylated RBBP5 levels were significantly greater in lesion samples than control samples, whereas total RBBP5 levels remained largely unchanged (Figure 5A). To further explore the correlation between HKDC1 and phosphorylated RBBP5, we performed immunohistochemistry (IHC) using serial sections of the same HCC tissues. The IHC images demonstrated elevated levels of both HKDC1 and pS497 in tumor tissues and indicated that areas with higher HKDC1 expression also showed strong staining for pS497 (Figure 5B). These findings suggest a strong correlation between HKDC1 and phosphorylated RBBP5.

To evaluate the clinical correlation of RBBP5 phosphorylation, we conducted an IHC analysis on 84 clinicopathologically characterized HCC cases. This cohort included 7 patients with stage I

(8.3%), 50 with stage II (59.5%), 20 with stage III (23.8%), and 7 with stage IV (8.3%) liver cancer, based on tumor, node, and metastasis staging. The analysis revealed abundant expression of phosphorylated RBBP5 in HCC tissues (Figure 5C). Quantitative analysis of IHC images revealed that pS497 levels were significantly higher in primary tumors than in normal tissues across all clinical stages I–IV (Figure 5D). Furthermore, pS497 levels were greater in late-stage HCC (stages III and IV) than in early-stage HCC (stages I and II), while total RBBP5 levels remained stable (Figure 5D). The Kaplan-Meier survival analysis demonstrated that patients whose HCC lesions had low levels of phosphorylated RBBP5 had significantly longer survival than those with high levels (Figure 5E). These results suggest that phosphorylated RBBP5 is positively correlated with advanced clinical stage and poor prognosis in patients with HCC. In conclusion, the phosphorylation of RBBP5 at Ser497 is a promising prognostic biomarker for HCC.

#### **DISCUSSION**

Accumulating evidence highlights the critical role of noncanonical functions of metabolic enzymes in the initiation and progression of cancer. These enzymes often exhibit alternative subcellular locations or unexpected activities beyond their traditional roles, affecting gene expression, cell cycle progression, and tumor microenvironment remodeling.<sup>3,4</sup> Some metabolic enzymes, typically known for transferring phosphate to metabolites, can also function as protein kinases that phosphorylate substrate proteins.<sup>3,41</sup> Our previous study demonstrated that the glycolytic enzyme HKDC1 promotes tumor immune evasion by associating with the cytoskeletal protein ACAT2 and stimulating STAT1 activation independently of its HK activity.<sup>15</sup> Here, we further revealed that nuclear-localized HKDC1 functions as a protein kinase, phosphorylating RBBP5 at the Ser497 site in liver cancer cells. This action enhances gene transcription and tumor cell proliferation. This noncanonical function significantly broadens our understanding of the direct role of HKDC1 in cancer proliferation.

HKDC1, a HK isozyme, shares high homology with HK1 and HK2 but has the lowest catalytic activity,<sup>14</sup> highlighting the potential importance of its noncanonical functions. In this study, we found that HKDC1 exhibits nuclear localization with aberrant expression in HCC. Considering that HKDC1 is distributed in the nucleus in paracancerous tissues and HCC tissues, the nuclear localization of HKDC1 is probably an intrinsic property. Furthermore, we elucidated the function of nuclear HKDC1 and emphasized the protein kinase activity of HKDC1, which is independent of its HK activity, in HCC cells. Structural prediction and experimental validation revealed that both the N- and

(B) Representative IHC images of HKDC1, pS497, and total RBBP5 staining in serial sections. Scale bars, 100 μm.

(C) Representative IHC images of pS497 and total RBBP5 staining in normal liver tissue (normal) and HCC samples of different clinical stages (I–IV); scale bars, 100 and 20 μm as indicated.

(D) Statistical quantification of MOD values for pS497 and total RBBP5 staining in IHC assays between normal liver tissues and HCC specimens at clinical stages I–IV (healthy donors,  $n = 18$ ; patients with HCC, stage I [ $n = 7$  patients], II [ $n = 50$  patients], III [ $n = 20$  patients], and IV [ $n = 7$  patients]). MOD, mean optical density.

(E) Kaplan-Meier curves with univariate analyses of patients with low or high expression of pS497 (high pS497,  $n = 42$  patients; low pS497,  $n = 42$  patients) or total RBBP5 (high RBBP5,  $n = 42$  patients; low RBBP5,  $n = 42$  patients).

Data are presented as mean ± SD (D). Statistical significance was determined by two-tailed Student's t test (D) and log rank test (E).

C-terminal regions of HKDC1 possess protein kinase activity, with glycine-rich motifs in these terminals being crucial for the catalytic process. Importantly, these protein kinase sites differ from the glucose-binding site (S602) and ATP-binding site (D654) of HKDC1, which are involved in its HK activity.<sup>15</sup> Additionally, HKDC1 failed to promote cell proliferation when the protein kinase sites were mutated, suggesting the more essential role of protein kinase activity in HCC than HK activity. Considering the conservation of metabolic catalytic functions within the HK family, targeting the protein kinase function of HKDC1 may not interfere with glucose metabolism, potentially reducing cytotoxicity and side effects. Thus, we identified a potential kinase inhibitor for HKDC1 and revealed that the effects of dinaciclib on RBBP5 phosphorylation and H3K4me3 level are mediated through the inhibition of HKDC1. Our findings reveal the protein kinase activity of HKDC1 and suggest a promising strategy for the clinical treatment of HCC.

Our study demonstrated that HKDC1-mediated phosphorylation of RBBP5 increases MLL1 complex assembly and H3K4me3 modification. Previous research has indicated that post-translational modifications of the subunits of the MLL1 complex modulate the methyltransferase activity. For example, SUMOylation of RBBP5 inhibits MLL1 activity by disrupting its binding with ASH2L,<sup>42</sup> whereas phosphorylation of RBBP5 at Ser350 promotes its interaction with ASH2L and boosts MLL1 activity.<sup>43</sup> Despite these findings, the specific regulators of histone methylation in cancer progression and their impact on the substrate specificity of methyltransferases remain unclear. In our study, we demonstrated that HKDC1 phosphorylates RBBP5 at the Ser497 residue and enhances its interaction with MLL1, WDR5, and ASH2L, promoting complex assembly. MLL1 alone catalyzes the methylation of H3K4 to H3K4me1 and H3K4me2,<sup>44,45</sup> but it forms a core complex with RBBP5, ASH2L, and WDR5 to catalyze H3K4me3.<sup>18,46</sup> Thus, HKDC1-increased MLL1 complex assembly upregulates H3K4me3, without affecting H3K4me1 or H3K4me2. Analysis using CUT&Tag and RNA-seq revealed that HKDC1 and RBBP5 upregulate H3K4me3 levels in the promoter regions of 6,258 genes and the mRNA levels of 834 genes. As H3K4me3 is a marker of transcriptionally active promoters and many other regulators are involved in transcriptional and post-transcriptional progress, there is a discrepancy between the two gene sets. Notably, 321 genes were co-regulated by HKDC1 and RBBP5, particularly those related to mitosis. These findings suggest that HKDC1 is a novel regulator of gene transcription in liver cancer cells. We also explored the potential involvement of the HKDC1-phosphorylated RBBP5-H3K4me3 axis in cancer progression by examining the integrity of the MLL1 complex. Our results elucidate the mechanism by which HKDC1 promotes tumor cell proliferation and highlight that targeting the aberrant activation of the MLL1 complex by HKDC1 may restrict tumor growth.

Our analysis of clinical HCC samples revealed that both HKDC1 and the level of phosphorylated RBBP5 at Ser497 are significantly greater in tumor tissues than in adjacent noncancerous tissues. Furthermore, phosphorylated RBBP5 correlated positively with the clinical stage and poor prognosis of patients with HCC. Notably, pS497 is almost undetectable in adjacent

tissues, indicating that MLL1 activity is abnormally high in liver cancer. These findings suggest that pS497 could serve as a valuable biomarker for the clinical diagnosis of HCC. Additionally, except for the strong correlation between HKDC1 and RBBP5, previous studies have reported the increased levels of MLL1 in HCC. This emphasized the promotion of the HKDC1/phosphorylated RBBP5/MLL1 axis in HCC progression. In summary, this study highlights the protein kinase function of HKDC1 and elucidates the mechanism by which HKDC1-mediated phosphorylation of RBBP5 activates H3K4me3 and promotes gene transcription. These insights provide a potential strategy for the clinical treatment of HCC.

### Limitations of the study

Our study highlighted the protein kinase function of nuclear HKDC1 in phosphorylating RBBP5 and revealed its role in MLL1 complex assembly and global H3K4m3, thereby promoting HCC progression. Through *in vitro* screening and *in vivo* validation, we identified dinaciclib as a potential kinase inhibitor of HKDC1. However, there are several limitations to note. First, the mechanism underlying HKDC1's nuclear localization remains unclear. Further studies are required to elucidate the connection between HKDC1's subcellular localization and its dual enzymatic functions. This will provide insights into the regulatory mechanisms determining its metabolic or protein kinase activity. Second, while dinaciclib was identified as a potential HKDC1 inhibitor, further studies are warranted to evaluate the specific contribution of dinaciclib-mediated HKDC1 inhibition to its anti-tumor effects. Finally, the structure basis of dinaciclib binding to HKDC1 is unknown, limiting our understanding of its specificity and mechanism of HKDC1 inhibition. Future studies could focus on resolving the HKDC1-dinaciclib structure to inform the design of modified dinaciclib with improved specificity and therapeutic potential. Addressing these limitations will provide a more comprehensive understanding of HKDC1.

### RESOURCE AVAILABILITY

#### Lead contact

Further information and requests for resources and reagents should be directed to and will be fulfilled by the lead contact, Huafeng Zhang ([hzhang22@ustc.edu.cn](mailto:hzhang22@ustc.edu.cn)).

#### Materials availability

All cell lines and plasmids generated in this study are available from the [lead contact](#).

#### Data and code availability

- The mass spectrometry proteomics data have been deposited to the ProteomeXchange Consortium via PRIDE. The accession number is listed in the [key resources table](#).
- CUT&Tag data and RNA-seq data have been deposited to GEO. The accession numbers are listed in the [key resources table](#).
- This study does not report original code.
- Any additional information required to reanalyze the data reported in this paper is available from the [lead contact](#) upon request.

### ACKNOWLEDGMENTS

This work is supported in part by the National Key R&D Program of China (2022YFA1304504), the National Natural Science Foundation of

China (82430097, 32450194, 82192893, 82341013, 92357301, 82130087, and 82103186), the Strategic Priority Research Program of the Chinese Academy of Sciences (XDB0940101), and the Global Select Project (DJK-LX-2022001) of the Institute of Health and Medicine, Hefei Comprehensive National Science Center.

#### AUTHOR CONTRIBUTIONS

H.Z. and P.G. conceived the study and supervised the experiments. L.Y., S.S., H.Z., and P.G. designed the experiments. L.Y., S.S., Q.M., H. Lu, H. Liu, P.Z., Z.J., W.M., Y.S., Y.C., Z.Z., R.L., J.L., and S.-t.L. performed the experiments. P.G. provided constructive guidance and advice. H.Z. and L.Y. wrote the paper. All authors read and approved the manuscript.

#### DECLARATION OF INTERESTS

The authors declare no competing interests.

#### STAR★METHODS

Detailed methods are provided in the online version of this paper and include the following:

- **KEY RESOURCES TABLE**
- **EXPERIMENTAL MODEL AND SUBJECT PARTICIPANT DETAILS**
  - Cell culture
  - Animal studies
  - Human samples
- **METHOD DETAILS**
  - Plasmids and established stable cells
  - Western blot assay
  - Immunoprecipitation assay
  - Subcellular fractionation
  - Cell cycle assay
  - Expression and purification of recombinant proteins
  - Pull-down assay
  - *In vitro* kinase assay and *in vitro* kinase inhibitor library screening
  - Immunofluorescence staining and confocal microscopy
  - CUT&Tag sequencing and data analysis
  - qRT-PCR
  - RNA-seq analysis
  - ChIP-qRT-PCR
  - IHC staining
- **QUANTIFICATION AND STATISTICAL ANALYSIS**

#### SUPPLEMENTAL INFORMATION

Supplemental information can be found online at <https://doi.org/10.1016/j.celrep.2025.115250>.

Received: September 30, 2024

Revised: December 4, 2024

Accepted: January 10, 2025

Published: January 31, 2025

#### REFERENCES

1. Hanahan, D., and Weinberg, R.A. (2011). Hallmarks of Cancer: The Next Generation. *Cell* 144, 646–674. <https://doi.org/10.1016/j.cell.2011.02.013>.
2. Pavlova, N.N., Zhu, J., and Thompson, C.B. (2022). The hallmarks of cancer metabolism: Still emerging. *Cell Metabol.* 34, 355–377. <https://doi.org/10.1016/j.cmet.2022.01.007>.
3. Xu, D., Shao, F., Bian, X., Meng, Y., Liang, T., and Lu, Z. (2021). The Evolving Landscape of Noncanonical Functions of Metabolic Enzymes in Cancer and Other Pathologies. *Cell Metabol.* 33, 33–50. <https://doi.org/10.1016/j.cmet.2020.12.015>.
4. Pan, C., Li, B., and Simon, M.C. (2021). Moonlighting functions of metabolic enzymes and metabolites in cancer. *Mol. Cell* 81, 3760–3774. <https://doi.org/10.1016/j.molcel.2021.08.031>.
5. Yang, W., Xia, Y., Hawke, D., Li, X., Liang, J., Xing, D., Aldape, K., Hunter, T., Alfred Yung, W.K., and Lu, Z. (2012). PKM2 Phosphorylates Histone H3 and Promotes Gene Transcription and Tumorigenesis. *Cell* 150, 685–696. <https://doi.org/10.1016/j.cell.2012.07.018>.
6. Dasgupta, S., Rajapakshe, K., Zhu, B., Nikolai, B.C., Yi, P., Putluri, N., Choi, J.M., Jung, S.Y., Coarfa, C., Westbrook, T.F., et al. (2018). Metabolic enzyme PFKFB4 activates transcriptional coactivator SRC-3 to drive breast cancer. *Nature* 556, 249–254. <https://doi.org/10.1038/s41586-018-0018-1>.
7. Anastasiou, D., Yu, Y., Israelsen, W.J., Jiang, J.K., Boxer, M.B., Hong, B.S., Tempel, W., Dimov, S., Shen, M., Jha, A., et al. (2012). Pyruvate kinase M2 activators promote tetramer formation and suppress tumorigenesis. *Nat. Chem. Biol.* 8, 1008. <https://doi.org/10.1038/nchembio1212-1008b>.
8. Lv, L., Xu, Y.P., Zhao, D., Li, F.L., Wang, W., Sasaki, N., Jiang, Y., Zhou, X., Li, T.T., Guan, K.L., et al. (2013). Mitogenic and Oncogenic Stimulation of K433 Acetylation Promotes PKM2 Protein Kinase Activity and Nuclear Localization. *Mol. Cell* 52, 340–352. <https://doi.org/10.1016/j.molcel.2013.09.004>.
9. Patra, K.C., Wang, Q., Bhaskar, P.T., Miller, L., Wang, Z., Wheaton, W., Chandel, N., Laakso, M., Muller, W.J., Allen, E.L., et al. (2013). Hexokinase 2 Is Required for Tumor Initiation and Maintenance and Its Systemic Deletion Is Therapeutic in Mouse Models of Cancer. *Cancer Cell* 24, 213–228. <https://doi.org/10.1016/j.ccr.2013.06.014>.
10. DeWaal, D., Nogueira, V., Terry, A.R., Patra, K.C., Jeon, S.M., Guzman, G., Au, J., Long, C.P., Antoniewicz, M.R., and Hay, N. (2018). Hexokinase-2 depletion inhibits glycolysis and induces oxidative phosphorylation in hepatocellular carcinoma and sensitizes to metformin. *Nat. Commun.* 9, 446. <https://doi.org/10.1038/s41467-017-02733-4>.
11. Guo, D., Tong, Y., Jiang, X., Meng, Y., Jiang, H., Du, L., Wu, Q., Li, S., Luo, S., Li, M., et al. (2022). Aerobic glycolysis promotes tumor immune evasion by hexokinase2-mediated phosphorylation of IκBa. *Cell Metabol.* 34, 1312–1324.e6. <https://doi.org/10.1016/j.cmet.2022.08.002>.
12. Chen, X., Lv, Y., Sun, Y., Zhang, H., Xie, W., Zhong, L., Chen, Q., Li, M., Li, L., Feng, J., et al. (2019). PGC1β Regulates Breast Tumor Growth and Metastasis by SREBP1-Mediated HKDC1 Expression. *Front. Oncol.* 9, 290. <https://doi.org/10.3389/fonc.2019.00290>.
13. Chen, Q., Feng, J., Wu, J., Yu, Z., Zhang, W., Chen, Y., Yao, P., and Zhang, H. (2020). HKDC1 C-terminal based peptides inhibit extranodal natural killer/T-cell lymphoma by modulation of mitochondrial function and EBV suppression. *Leukemia* 34, 2736–2748. <https://doi.org/10.1038/s41375-020-0801-5>.
14. Pusec, C.M., De Jesus, A., Khan, M.W., Terry, A.R., Ludvik, A.E., Xu, K., Giancola, N., Pervaiz, H., Daviau Smith, E., Ding, X., et al. (2019). Hepatic HKDC1 Expression Contributes to Liver Metabolism. *Endocrinology* 160, 313–330. <https://doi.org/10.1210/en.2018-00887>.
15. Zhang, Y., Wang, M., Ye, L., Shen, S., Zhang, Y., Qian, X., Zhang, T., Yuan, M., Ye, Z., Cai, J., et al. (2024). HKDC1 promotes tumor immune evasion in hepatocellular carcinoma by coupling cytoskeleton to STAT1 activation and PD-L1 expression. *Nat. Commun.* 15, 1314. <https://doi.org/10.1038/s41467-024-45712-2>.
16. Chen, Y., Ren, B., Yang, J., Wang, H., Yang, G., Xu, R., You, L., and Zhao, Y. (2020). The role of histone methylation in the development of digestive cancers: a potential direction for cancer management. *Signal Transduct Tar* 5, 143. <https://doi.org/10.1038/s41392-020-00252-1>.
17. Ding, X., He, M., Chan, A.W.H., Song, Q.X., Sze, S.C., Chen, H., Man, M.K.H., Man, K., Chan, S.L., Lai, P.B.S., et al. (2019). Genomic and Epigenomic Features of Primary and Recurrent Hepatocellular Carcinomas. *Gastroenterology* 157, 1630–1645.e6. <https://doi.org/10.1053/j.gastro.2019.09.005>.

18. Dou, Y., Milne, T.A., Ruthenburg, A.J., Lee, S., Lee, J.W., Verdine, G.L., Allis, C.D., and Roeder, R.G. (2006). Regulation of MLL1 H3K4 methyltransferase activity by its core components. *Nat. Struct. Mol. Biol.* 13, 713–719. <https://doi.org/10.1038/nsmb1128>.
19. Southall, S.M., Wong, P.S., Odbo, Z., Roe, S.M., and Wilson, J.R. (2009). Structural Basis for the Requirement of Additional Factors for MLL1 SET Domain Activity and Recognition of Epigenetic Marks. *Mol. Cell* 33, 181–191. <https://doi.org/10.1016/j.molcel.2008.12.029>.
20. Shen, S.M., Zhang, C., Ge, M.K., Dong, S.S., Xia, L., He, P., Zhang, N., Ji, Y., Yang, S., Yu, Y., et al. (2019). PTEN $\alpha$  and PTEN $\beta$  promote carcinogenesis through WDR5 and H3K4 trimethylation. *Nat. Cell Biol.* 21, 1436–1448. <https://doi.org/10.1038/s41556-019-0409-z>.
21. Zhai, X., and Brownell, J.E. (2021). Biochemical perspectives on targeting KMT2 methyltransferases in cancer. *Trends Pharmacol. Sci.* 42, 688–699. <https://doi.org/10.1016/j.tips.2021.05.002>.
22. Takahashi, Y.H., Westfield, G.H., Oleskie, A.N., Trievle, R.C., Shilatifard, A., and Skiniotis, G. (2011). Structural analysis of the core COMPASS family of histone H3K4 methylases from yeast to human. *P Natl Acad Sci USA* 108, 20526–20531. <https://doi.org/10.1073/pnas.1109360108>.
23. Takeda, S., Liu, H., Sasagawa, S., Dong, Y., Trainor, P.A., Cheng, E.H., and Hsieh, J.J. (2013). HGF-MET signals via the MLL-ETS2 complex in hepatocellular carcinoma. *J. Clin. Invest.* 123, 3154–3165. <https://doi.org/10.1172/JCI65566>.
24. Zhu, J., Sammons, M.A., Donahue, G., Dou, Z., Vedadi, M., Getlik, M., Barssy-Lovejoy, D., Al-Awar, R., Katona, B.W., Shilatifard, A., et al. (2015). Gain-of-function p53 mutants co-opt chromatin pathways to drive cancer growth. *Nature* 525, 206–211. <https://doi.org/10.1038/nature15251>.
25. Sung, W.K., Zheng, H., Li, S., Chen, R., Liu, X., Li, Y., Lee, N.P., Lee, W.H., Ariyaratne, P.N., Tennakoon, C., et al. (2012). Genome-wide survey of recurrent HBV integration in hepatocellular carcinoma. *Nat. Genet.* 44, 765–769. <https://doi.org/10.1038/ng.2295>.
26. Chang, Y.S., Tu, S.J., Chen, H.D., Hsu, M.H., Chen, Y.C., Chao, D.S., Chung, C.C., Chou, Y.P., Chang, C.M., Lee, Y.T., et al. (2023). Integrated genomic analyses of hepatocellular carcinoma. *Hepatol. Int.* 17, 97–111. <https://doi.org/10.1007/s12072-022-10455-z>.
27. Li, X., Jiang, Y., Meisenhelder, J., Yang, W., Hawke, D.H., Zheng, Y., Xia, Y., Aldape, K., He, J., Hunter, T., et al. (2016). Mitochondria-Translocated PGK1 Functions as a Protein Kinase to Coordinate Glycolysis and the TCA Cycle in Tumorigenesis. *Mol. Cell* 61, 705–719. <https://doi.org/10.1016/j.molcel.2016.02.009>.
28. Xu, D., Wang, Z., Xia, Y., Shao, F., Xia, W., Wei, Y., Li, X., Qian, X., Lee, J.H., Du, L., et al. (2020). The gluconeogenic enzyme PCK1 phosphorylates INSIG1/2 for lipogenesis. *Nature* 580, 530–535. <https://doi.org/10.1038/s41586-020-2183-2>.
29. Taylor, S.S., and Kornev, A.P. (2011). Protein kinases: evolution of dynamic regulatory proteins. *Trends Biochem. Sci.* 36, 65–77. <https://doi.org/10.1016/j.tibs.2010.09.006>.
30. Leroux, A.E., and Biondi, R.M. (2020). Renaissance of Allostery to Disrupt Protein Kinase Interactions. *Trends Biochem. Sci.* 45, 27–41. <https://doi.org/10.1016/j.tibs.2019.09.007>.
31. Patel, A., Dharmarajan, V., Vought, V.E., and Cosgrove, M.S. (2009). On the Mechanism of Multiple Lysine Methylation by the Human Mixed Lineage Leukemia Protein-1 (MLL1) Core Complex. *J. Biol. Chem.* 284, 24242–24256. <https://doi.org/10.1074/jbc.M109.014498>.
32. Han, J., Li, T., Li, Y., Li, M., Wang, X., Peng, C., Su, C., Li, N., Li, Y., Xu, Y., and Chen, Y. (2019). The internal interaction in RBBP5 regulates assembly and activity of MLL1 methyltransferase complex. *Nucleic Acids Res.* 47, 10426–10438. <https://doi.org/10.1093/nar/gkz819>.
33. Kim, T.H., Barrera, L.O., Zheng, M., Qu, C., Singer, M.A., Richmond, T.A., Wu, Y., Green, R.D., and Ren, B. (2005). A high-resolution map of active promoters in the human genome. *Nature* 436, 876–880. <https://doi.org/10.1038/nature03877>.
34. Barski, A., Cuddapah, S., Cui, K., Roh, T.Y., Schones, D.E., Wang, Z., Wei, G., Chepelev, I., and Zhao, K. (2007). High-resolution profiling of histone methylation in the human genome. *Cell* 129, 823–837. <https://doi.org/10.1016/j.cell.2007.05.009>.
35. Attwood, M.M., Fabbro, D., Sokolov, A.V., Knapp, S., and Schiöth, H.B. (2021). Trends in kinase drug discovery: targets, indications and inhibitor design. *Nat. Rev. Drug Discov.* 20, 798. <https://doi.org/10.1038/s41573-021-00303-4>.
36. Otto, T., and Sicinski, P. (2017). Cell cycle proteins as promising targets in cancer therapy. *Nat. Rev. Cancer* 17, 93–115. <https://doi.org/10.1038/nrc.2016.138>.
37. Ghia, P., Scarfò, L., Perez, S., Pathiraja, K., Derosier, M., Small, K., McCrary Sisk, C., and Patton, N. (2017). Efficacy and safety of dinaciclib vs ofatumumab in patients with relapsed/refractory chronic lymphocytic leukemia. *Blood* 129, 1876–1878. <https://doi.org/10.1182/blood-2016-10-748210>.
38. Stephenson, J.J., Nemunaitis, J., Joy, A.A., Martin, J.C., Jou, Y.M., Zhang, D., Statkevich, P., Yao, S.L., Zhu, Y., Zhou, H., et al. (2014). Randomized phase 2 study of the cyclin-dependent kinase inhibitor dinaciclib (MK-7965) versus erlotinib in patients with non-small cell lung cancer. *Lung Cancer* 83, 219–223. <https://doi.org/10.1016/j.lungcan.2013.11.020>.
39. Mita, M.M., Joy, A.A., Mita, A., Sankhala, K., Jou, Y.M., Zhang, D., Statkevich, P., Zhu, Y., Yao, S.L., Small, K., et al. (2014). Randomized Phase II Trial of the Cyclin-Dependent Kinase Inhibitor Dinaciclib (MK-7965) Versus Capecitabine in Patients With Advanced Breast Cancer. *Clin. Breast Cancer* 14, 169–176. <https://doi.org/10.1016/j.clbc.2013.10.016>.
40. Grebien, F., Vedadi, M., Getlik, M., Giambruno, R., Grover, A., Avellino, R., Skucha, A., Vittori, S., Kuznetsova, E., Smil, D., et al. (2015). Pharmacological targeting of the Wdr5-MLL interaction in C/EBP $\alpha$  N-terminal leukemia. *Nat. Chem. Biol.* 11, 571–578. <https://doi.org/10.1038/nchembio.1859>.
41. Meng, Y., Guo, D., Lin, L., Zhao, H., Xu, W., Luo, S., Jiang, X., Li, S., He, X., Zhu, R., et al. (2024). Glycolytic enzyme PFKL governs lipolysis by promoting lipid droplet-mitochondria tethering to enhance  $\beta$ -oxidation and tumor cell proliferation. *Nat. Metab.* 6, 1092–1107. <https://doi.org/10.1038/s42255-024-01047-2>.
42. Nayak, A., Viale-Bouroncle, S., Morsczeck, C., and Muller, S. (2014). The SUMO-Specific Isopeptidase SENP3 Regulates MLL1/MLL2 Methyltransferase Complexes and Controls Osteogenic Differentiation. *Mol. Cell* 55, 47–58. <https://doi.org/10.1016/j.molcel.2014.05.011>.
43. Zhang, P., Chaturvedi, C.P., Tremblay, V., Cramet, M., Brunzelle, J.S., Skiniotis, G., Brand, M., Shilatifard, A., and Couture, J.F. (2015). A phosphorylation switch on RbBP5 regulates histone H3 Lys4 methylation. *Gene Dev.* 29, 123–128. <https://doi.org/10.1101/gad.254870.114>.
44. Milne, T.A., Briggs, S.D., Brock, H.W., Martin, M.E., Gibbs, D., Allis, C.D., and Hess, J.L. (2002). MLL targets SET domain methyltransferase activity to gene promoters. *Mol. Cell* 10, 1107–1117. [https://doi.org/10.1016/S1097-2765\(02\)00741-4](https://doi.org/10.1016/S1097-2765(02)00741-4).
45. Nakamura, T., Mori, T., Tada, S., Krajewski, W., Rozovskaia, T., Wassell, R., Dubois, G., Mazo, A., Croce, C.M., and Canaani, E. (2002). ALL-1 is a histone methyltransferase that assembles a supercomplex of proteins involved in transcriptional regulation. *Mol. Cell* 10, 1119–1128. [https://doi.org/10.1016/S1097-2765\(02\)00740-2](https://doi.org/10.1016/S1097-2765(02)00740-2).
46. Schneider, J., Wood, A., Lee, J.S., Schuster, R., Dueker, J., Maguire, C., Swanson, S.K., Florens, L., Washburn, M.P., and Shilatifard, A. (2005). Molecular regulation of histone H3 trimethylation by COMPASS and the regulation of gene expression. *Mol. Cell* 19, 849–856. <https://doi.org/10.1016/j.molcel.2005.07.024>.
47. Zhou, Y., Zhou, B., Pache, L., Chang, M., Khodabakhshi, A.H., Tanaseichuk, O., Benner, C., and Chanda, S.K. (2019). Metascape provides a biologist-oriented resource for the analysis of systems-level datasets. *Nat. Commun.* 10, 1523. <https://doi.org/10.1038/s41467-019-09234-6>.

## STAR★METHODS

### KEY RESOURCES TABLE

REAGENT or RESOURCE	SOURCE	IDENTIFIER
<b>Antibodies</b>		
Rabbit Polyclonal Anti-HKDC1	Proteintech	Cat# 25874-1-AP; RRID: AB_2880279
Rabbit Polyclonal Anti-HKDC1	Abclonal	Cat# E19270; RRID: AB_3675515
Rabbit Polyclonal Anti-RBBP5-pS497	Abclonal	Cat# E20544; RRID: AB_3675516
Mouse Monoclonal Anti-HK1	Santa Cruz	Cat# sc-46695; RRID: AB_627721
Mouse Monoclonal Anti-HK2	Santa Cruz	Cat# sc-374091; RRID: AB_10917915
Rabbit Monoclonal Anti-RBBP5	CST	Cat# 13171; RRID: AB_2714169
Mouse Monoclonal Anti-WDR5	Santa Cruz	Cat# sc-393080; RRID: AB_3331659
Rabbit Polyclonal Anti-ASH2L	Proteintech	Cat# 12331-1-AP; RRID: AB_2059837
Rabbit Monoclonal Anti-MLL1c	CST	Cat# 14197; RRID: AB_2688010
Rabbit Monoclonal Anti-H3K4me3	CST	Cat# 9751; RRID: AB_2616028
Rabbit Polyclonal Anti-H3	Proteintech	Cat# 17168-1-AP; RRID: AB_2716755
Rabbit Monoclonal Anti-Thiophosphate ester	Abcam	Cat# ab92570; RRID: AB_10562142
Mouse Monoclonal Anti-Phosphoserine	Millipore	Cat# 05-1000; RRID: AB_916368
Rabbit Monoclonal Anti-ATAD5	Sangon	Cat# D261469; RRID: AB_3674288
Rabbit Monoclonal Anti-CENPE	Abcam	Cat# ab133583; RRID: AB_2910100
Rabbit Monoclonal Anti-CDC27	Sangon	Cat# D261541; RRID: AB_3674296
Rabbit Monoclonal Anti-KIF14	Sangon	Cat# D163049; RRID: AB_3674320
Rabbit Polyclonal Anti-KNL1	Abclonal	Cat# A13108; RRID: AB_2759957
Rabbit Monoclonal Anti-NEK7	CST	Cat# 3057; RRID: AB_2150676
Mouse Monoclonal Anti-Flag-M2	Sigma	Cat# F1804; RRID: AB_262044
Monoclonal Anti-HA-tag-HRP-conjugate	CST	Cat# 2999; RRID: AB_1264166
Rabbit Polyclonal Anti-GST-tag	Proteintech	Cat# 10000-0-AP; RRID: AB_11042316
Mouse Monoclonal Anti-His-tag	Proteintech	Cat# 66005-1-Ig; RRID: AB_11232599
Mouse Monoclonal Anti-β-Actin	Proteintech	Cat# 66009-1-Ig; RRID: AB_2687938
Rabbit Polyclonal Anti-LaminB1	Proteintech	Cat# 12987-1-AP; RRID: AB_2136290
Mouse Monoclonal Anti-α-Tubulin	Proteintech	Cat# 66031-1-Ig; RRID: AB_11042766
Rabbit Polyclonal Anti-Calnexin	Proteintech	Cat# 10427-2-AP; RRID: AB_2069033
<b>Bacterial and virus strains</b>		
Bacteria: DH5a	Tsingke	Cat# TSC-C01
Bacteria: Rosetta (DE3)	Tsingke	Cat# TSC-E04
<b>Biological samples</b>		
Paired HCC and noncancerous tissues	The First Affiliated Hospital of USTC	N/A
<b>Chemicals, peptides, and recombinant proteins</b>		
Kinase inhibitor library	Topscience	Cat# L1600
Dinaciclib	Topscience	Cat# T1912
OICR-9429	Topscience	Cat# T6916
Polybrene	Sigma	Cat# H9268
Puromycin	Sigma	Cat# P8833
PEI	Polysciences	Cat# 23966-2
Penicillin-streptomycin	HyClone	Cat# SV30010
Certified Fetal Bovine Serum	VivaCell	Cat# C04001-500

(Continued on next page)

**Continued**

REAGENT or RESOURCE	SOURCE	IDENTIFIER
<b>Critical commercial assays</b>		
Bradford Assay Kit	Sangon Biotech	Cat# C503041
Hyperactive Universal CUT&Tag Assay Kit	Vazyme	Cat# TD903-01
HiScript III RT SuperMix	Vazyme	Cat# R323
EZ-ChIP Kit	Millipore	Cat# 17-371
ADP-Glo™ Max Assay Kit	Promega	Cat# V6930
Matrigel	BD	Cat# 356234
<b>Deposited data</b>		
WB source data	This paper; Mendeley data	<a href="https://data.mendeley.com/datasets/r2n58xg54s/1">https://data.mendeley.com/datasets/r2n58xg54s/1</a>
The mass spectrometry proteomics data	This paper	PRIDE: PXD059464
CUT&Tag data	This paper	GEO: GSE275531
RNA-seq data	This paper	GEO: GSE275644
<b>Experimental models: Cell lines</b>		
Human: HEK293T	ATCC	Cat# CRL-3216
Human: Hep3B	ATCC	Cat# HB-8064
Human: PLC	ATCC	Cat# CRL-8024
<b>Experimental models: Organisms/strains</b>		
Nude	Shanghai SLAC Laboratory Animal Co., China	N/A
C57BL/6	Shanghai SLAC Laboratory Animal Co., China	N/A
<b>Oligonucleotides</b>		
For shRNA targeting sequences, see <a href="#">Table S1</a>	This manuscript	N/A
For qRT-PCR primers, see <a href="#">Table S2</a>	This manuscript	N/A
For ChIP-qRT-PCR primers, see <a href="#">Table S3</a>	This manuscript	N/A
<b>Recombinant DNA</b>		
Plasmid: pSin-3xflag-EF1 $\alpha$	This manuscript	N/A
Plasmid: pLKO.1 puro	Sigma	Cat# SHC001
Plasmid: pET22b-6xHis	This manuscript	N/A
Plasmid: pGEX-4T1-GST	This manuscript	N/A
Plasmid: pT/Caggs-NRASV12	Addgene	Cat# 20205
Plasmid: pT2/shp53/GFP4	Addgene	Cat# 20208
Plasmid: PT2/C-Luc//PGK-SB13	Addgene	Cat# 20207
Gene mutants see plasmids part in Methods details	This manuscript	N/A
<b>Software and algorithms</b>		
FlowJo	Software	<a href="https://www.flowjo.com">https://www.flowjo.com</a>
ZEISS	Software	<a href="https://www.zeiss.com">https://www.zeiss.com</a>
Integrative Genomics Viewer	Software	<a href="https://www.igv.org">https://www.igv.org</a>
TissueFAXS	Software	<a href="https://tissueugnostics.com/">https://tissueugnostics.com/</a>
HistoQuest	Software	<a href="https://tissueugnostics.com/">https://tissueugnostics.com/</a>
GraphPad Prism 8	Software	<a href="https://www.graphpad.com/">https://www.graphpad.com/</a>
ImageJ	Software	<a href="https://imagej.nih.gov/ij/">https://imagej.nih.gov/ij/</a>

## EXPERIMENTAL MODEL AND SUBJECT PARTICIPANT DETAILS

### Cell culture

All cell lines were purchased from the American Type Culture Collection (ATCC). Human Hep3B, PLC, HepG2, A549, CALU3, MDA-MB-231, MDA-MB-468, and HEK293T cells were cultured in DMEM (12800082, Gibco) supplemented with 10% fetal bovine serum (FBS) (C04001, VivaCell) and 1% penicillin/streptomycin (E607011, Sangon Biotech). THLE3 cells were maintained in Bronchial Epithelial Cell Growth Medium (BEGM) (CC-3170, Walkersville) containing 10% FBS. All cells were incubated at 37°C in a humidified

atmosphere with 5% CO<sub>2</sub>. All cell lines were authenticated by STR analysis and validated to be free of mycoplasma contamination before usage in this study.

### Animal studies

All animal studies received approval from the Animal Research Ethics Committee at the University of Science and Technology of China. The construction of *Hkdc1*<sup>-/-</sup> mice was described previously.<sup>15</sup> WT C57BL/6 mice and nude mice were purchased from Shanghai SLAC Laboratory Animal Co., China. Only male mice were used to perform experiments, but there was no sex-based analysis in these studies.

For the orthotopic liver cancer model, 25 µg of plasmids expressing NRAS<sup>G12V</sup>, 29 µg of plasmids expressing shP53, and 56 µg of plasmids expressing SB13 suspended in normal saline solution were delivered to 8-week-old WT or *Hkdc1*<sup>-/-</sup> C57BL/6 mice via hydrodynamic tail vein injection (HDI). Mice were sacrificed approximately 2 months after the injection.

In xenograft experiments, 3×10<sup>6</sup> Hep3B cells stably expressing HKDC1, HKDC1<sup>S602A</sup>, RBBP5, or RBBP5<sup>S497D</sup> were injected subcutaneously into 6-week-old male nude mice, followed by the indicated treatment. Tumor-bearing mice were randomly divided into different groups before treatment. The tumor volumes were measured using digital calipers every 3 days and calculated using the formula: Tumor volume (mm<sup>3</sup>) = length (mm) × width (mm) × depth (mm) × 0.52. Dinaciclib was diluted (Topscience) in a solution containing 10% DMSO, 40% PEG300, and 5% Tween 80. OICR-9429 (Topscience) was diluted in a solution containing 5% DMSO, 40% PEG300, and 2% Tween 80. Mice were treated with Dinaciclib (20 mg per kg) or OICR-9429 (50 mg per kg) every 3 days by intraperitoneal injection, starting one week after inoculation.

### Human samples

The 12 pairs of HCC tissues and corresponding para-cancerous tissues were randomly selected for protein extraction to analyze the level of HKDC1, pS497 and RBBP5. Formalin-fixed, paraffin-embedded primary HCC specimens from 84 patients were randomly selected for IHC staining. The clinical data and pathological characteristics for 84 patients, including age, gender, tumor size, tumor lymph node involvement, serum alpha-fetoprotein levels, hepatitis B surface antigen status, vascular invasion, and liver cirrhosis, were recorded. Detailed patient data and the correlation analysis are shown in [Tables S1–S4](#). Our results do not suggest any apparent influence of sex or gender on the findings. Tumor clinical stages were determined according to the fifth edition of the American Joint Committee on Cancer/International Union Against Cancer (AJCC/UICC) tumor/lymph node metastasis/distal metastasis (TNM) classification system. For using these clinical materials for research purposes, prior patients' written informed consents and approval from the Institutional Research Ethics Committee of the First Affiliated Hospital of the University of Science and Technology of China were obtained. The ethical approval number is 2021-A(H)-039.

## METHOD DETAILS

### Plasmids and established stable cells

Lentiviral shRNAs targeting HKDC1 and RBBP5 in the pLKO.1 vector was commercially purchased (Sigma-Aldrich). These shRNAs were designed to target the 3'UTR of HKDC1 and RBBP5. The sequences for the shRNAs are detailed in [Table S5](#). HKDC1, HKDC1<sup>S602A</sup>, HKDC1<sup>KD</sup>, truncation mutants of HKDC1, HK1, HK2, WDR5, ASH2L, RBBP5, RBBP5<sup>S497A</sup>, RBBP5<sup>S497D</sup>, truncation mutants of RBBP5, and the WIN and SET domains of six MLL family proteins were subcloned into the pSin-EF2 vector with a FLAG tag at the C-terminal. HKDC1 was also subcloned into the pSin-HA vector. Each lentiviral plasmid was co-transfected with packaging plasmids pMD2.G and pSPAX into HEK293T cells using PEI (23966-2, Polysciences). Viral supernatant was collected 48 h after transfection, filtered (SLGP033RS, Millipore), and added to Hep3B or PLC cells in the presence of 8 µg/mL polybrene (H9268, Sigma-Aldrich). The stable cells were selected with 0.5–1 µg/mL puromycin (P8833, Sigma-Aldrich).

### Western blot assay

Cells were lysed in RIPA buffer (50 mM Tris-Cl, pH 8.0, 150 mM NaCl, 5 mM EDTA, 0.1% SDS, 1% NP-40) supplemented with protease inhibitor cocktails (5056489001, Roche) for 45 min. Equal amounts of proteins were fractionated by SDS-PAGE. Primary antibodies against HKDC1, HK1, HK2, RBBP5, ASH2L, WDR5, MLL1c, H3K4me3, H3, Thiophosphate, p-Ser, ATAD5, CENPE, CDC27, KIF14, KNL1, NEK7, β-actin, Flag, Lamin B, GAPDH, and α-Tubulin are listed in the key resources table. HRP-conjugated anti-rabbit and anti-mouse secondary antibodies (1191, 1676, Bio-Brd) were used. The signal was detected using Western ECL Substrate (Bio-Brd).

### Immunoprecipitation assay

For immunoprecipitation, cells were lysed in IP buffer (20 mM Tris-HCl, pH 7.5, 150 mM NaCl, 1.5 mM MgCl<sub>2</sub>, 2 mM EDTA, 1.0% NP-40) supplemented with protease inhibitor cocktail for 1–2 h on ice, and centrifuged at 12,000 g for 10 min at 4°C. The supernatants were incubated with the indicated antibody overnight at 4°C, followed by incubation with protein A/G conjugated beads (53133, Thermo Fisher) for 2 h. Beads were then washed with IP buffer and boiled in 2×SDS-loading buffer. Protein samples were analyzed by Western blotting.

### Subcellular fractionation

Cells were lysed in nuclear buffer (1 mM KH<sub>2</sub>PO<sub>4</sub>, pH 7.4, 150 mM NaCl, 5 mM MgCl<sub>2</sub>, 0.6% Triton X-100) supplemented with PMSF and DTT for 10–20 min on ice. After centrifugation at 1500g for 10 min at 4°C, the supernatant contained cytoplasmic proteins and the pellet contained nuclear proteins. Using sonication, the nuclear pellet was further lysed in nuclear lysis buffer (50 mM Tris-HCl, pH 7.5, 500 mM NaCl, 1 mM EDTA, 0.2% NP-40, 5 mM glycerol, 10 mM 2-ME). Protein concentration was determined using a BCA assay kit. Protein samples were analyzed by Western blotting.

### Cell cycle assay

Hep3B cells were trypsinized and combined with floating cells. Cells were washed with cold phosphate-buffered saline (PBS) and fixed with ice-cold 70% ethanol for 30 min at room temperature. After fixation, cells were washed three times and suspended in a staining solution containing 20 mg/mL propidium iodide and 200 mg/mL RNase A followed by incubation in the dark for 30 min at 4°C. Following incubation, cells were washed twice and then filtered through a 200-mesh filter before analysis using a FACScan flow cytometer (BD Biosciences) and FlowJo software (v 10.3).

### Expression and purification of recombinant proteins

The cDNAs encoding HKDC1, its truncations, and its mutants, as well as RBBP5 and its mutants, were subcloned into the pET-22b vector with a His tag at the C-terminal. Similarly, cDNAs encoding RBBP5, its truncations, DPY30, WDR5, and ASH2L were subcloned into the PGEX-4T1 vector with a GST tag at the N-terminal. All plasmids were transfected into *Escherichia coli* Rosetta (DE3) (Tsingke Biological Technology) and induced protein expression with 0.5 mM IPTG. After collecting the bacterial cells, the proteins were subjected to ultrasonic lysis. The His-tagged proteins were purified using Ni-NTA Agarose (C600033, Sangon Biotech), and the GST-fused proteins were purified using Glutathione Sepharose 4B (17075601, GE Life).

### Pull-down assay

Purified His-tagged proteins and GST-fused proteins were incubated in pull-down buffer (50 mM Tris, pH 7.5, 150 mM NaCl, 0.5% Triton X-100, 5 mM DTT) for 30 min. After incubation, the beads were washed with pull-down buffer and boiled at 100°C. Protein samples were analyzed by Western blotting.

### In vitro kinase assay and in vitro kinase inhibitor library screening

For the *in vitro* kinase assay, purified His-RBBP5 was incubated with purified His-HKDC1 in 50 µL kinase buffer (25 mM Tris-HCl, pH 7.4, 10 mM MgCl<sub>2</sub>, 5 mM glycerol, 1 mM Na<sub>3</sub>VO<sub>4</sub>, 1 mM DTT) supplemented with 100 µM ATP-γ-S (ab138911, Abcam) for 30 min at 37 °C. The reaction was terminated by adding 40 mM EDTA and incubating for 5 min at 37 °C. The samples were alkylated with 50 mM PNBM (ab138910, Abcam) for 1 to 2 h at room temperature and then analyzed by Western blotting.

For *in vitro* kinase inhibitor library screening, 100 µg of purified His-RBBP5 was incubated with 200 µg of purified His-HKDC1 in 20 µL kinase buffer supplemented with 30 µM inhibitors from the kinase inhibitor library (L1600, Topscience). The reaction was initiated by adding 10 µM ATP and then incubated for 30 min at 37 °C. The amount of ADP produced in the reactions was measured using the ADP-Glo Max Assay kit (V6930, Promega), which indicates kinase activity.

### Immunofluorescence staining and confocal microscopy

Cells were fixed with 4% paraformaldehyde, blocked with PBS containing 5% BSA, and incubated with anti-Flag antibody (1:100). Anti-mouse secondary antibodies conjugated to FITC (green). The nuclei were stained with DAPI (D9542, Sigma). Images were acquired using a fluorescent confocal microscope (ZEISS710) and analyzed with ZEN microscope imaging software (ZEISS).

### CUT&Tag sequencing and data analysis

For CUT&Tag assay, Hyperactive Universal CUT&Tag Assay Kit (TD903-01, Vazyme) was used according to the manufacturer's instructions. An anti-H3K4me3 antibody was used to pull down DNA-protein complexes. Sequencing was conducted at Novogene (Tianjin, China) on the Illumina NovaSeq platform. Sequenced reads were aligned to the human genome hg19 using Bowtie2 (v 2.4.2). The aligned reads were removed with Picard MarkDuplicates. The deduplicated BAM files were normalized to the total aligned reads (reads per million, RPM) with the BamCoverage command from DeepTools (v 3.4.3). Macs2 (v 2.2.6) was used for peak calling. Peaks were classified based on their location using UCSC annotation data and categorized into the following genome regions: intergenic, introns, downstream, upstream, and exons. The gene traces were visualized using the Integrative Genomics Viewer. Data were visualized using plotHeatmap in DeepTools.

### qRT-PCR

Total RNA was isolated using TRIzol (15596-018, Thermo Fisher) followed by reverse transcription with HiScript III RT SuperMix for qPCR (Vazyme). qRT-PCR was performed using SYBR Green master mix (Vazyme) on a Bio-Rad iCycler. All samples were normalized to 18S rRNA. The primer sequences used are shown in Table S6. The fold change in target mRNA expression was calculated based on the threshold cycle (Ct) values, where  $\Delta Ct = Ct_{target} - Ct_{18S}$  and  $\Delta(\Delta Ct) = \Delta Ct_{Control} - \Delta Ct_{Indicated\ condition}$ .

**RNA-seq analysis**

Total RNA was extracted using TRIzol according to the manufacturer's instructions. The RNA integrity was assessed with the Agilent Bioanalyzer 2100. Libraries were generated using the NEB Next Ultra RNA Library Prep Kit for Illumina (NEB). Sequencing was conducted on the Illumina NovaSeq platform by Novogene. Reads were aligned to the human genome hg19 using Hisat2 (v 2.2.1), transcripts were assembled with Stringtie (v 1.3.4), and gene differential expression analysis was carried out with the DESeq2 (v 1.28.1). Pathway enrichment analysis were carried out using Metascape (v 3.5).<sup>47</sup>

**ChIP-qRT-PCR**

For ChIP assay, EZ-ChIP Kit (17–371, Millipore) was used according to the manufacturer's instructions. DNA was immunoprecipitated with an anti-H3K4me3 or control IgG antibody. Purified DNA was quantified using qRT-PCR. The primer sequences used are listed in [Table S7](#).

**IHC staining**

Samples were dewaxed using xylene and rehydrated with graded ethanol. Following antigen retrieval, sections were incubated in 0.3% hydrogen peroxide for 10 min and then in normal goat serum for 15 min. Anti-RBBP5 or anti-pS497 antibodies were used to incubate at room temperature for 4 to 6 h, followed by the application of a secondary antibody. Sections were developed using DAB Chromogen dilution solution. The IHC staining was quantitatively analyzed using TissueFAXS (TissueGnostic) and HistoQuest (v 4.0) (TissueGnostic). The mean optical density (MOD) was verified by analysis of ten staining fields from each section, and the differences between groups were compared using a Two-tailed unpaired Student's t-test.

**QUANTIFICATION AND STATISTICAL ANALYSIS**

The data were presented as mean  $\pm$  SD from three independent experiments and analyzed using Graph Prism 8.0 software. Student's t-test was used to compare the two groups. Two-tailed unpaired Student's t-test and one- or two-way analysis of variance (ANOVA) were used to calculate *p* values. Kaplan-Meier curves were used to determine survival analysis and differences in the survival rates were compared with the log rank test. The relationship between expression of RBBP5 or pS497 and clinicopathological characteristics was analyzed by a chi-square test or spearman. Statistical significance was indicated with \* (*p* < 0.05; \*\**p* < 0.01; \*\*\**p* < 0.001; n.s.: not significant) unless otherwise specified. All statistical details of the experiments can be found in the figure legends or [Tables S2](#) and [S3](#).